Multichannel Blind Image Deconvolution For Sparse Molecular Imaging

Umer Javeed

112-FET/MSEE/F07

MS Electronic Engineering

Department of Electronic Engineering

Faculty of Engineering and Technology

International Islamic University, Islamabad.

2009

Multichannel Blind Image Deconvolution For Sparse Molecular Imaging

TC 5947

Umer Javeed

112-FET/MSEE/F07

This dissertation is submitted as partial fulfillment of degree

MS Electronic Engineering

Department of Electronic Engineering

Faculty of Engineering and Technology

International Islamic University, Islamabad.

2009

Certificate of Approval

It is certified that awe have read the project report submitted by **Umer Javeed [112-FET/MSEE/F07]**. It is our judgment that this project Is of sufficient standard to warrant its acceptance by International Islamic University, Islamabad for MS(EE) Degree in Electronic Engineering.
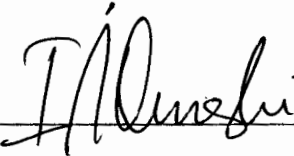

Supervisor
Dr. Tanweer Ahmed Cheema
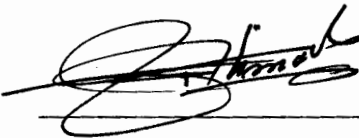Assistant Professor,
FET, IIU, Islamabad.

External Examiner
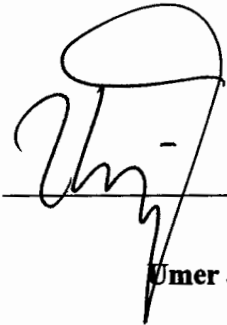Dr. I. M. Qureshi
Professor,
Air University.

Internal Examiner
Dr. Bashir Ahmad Zahir
Assistant Professor,
FET, IIU, Islamabad.

Declaration

I certify that except where due acknowledgments has been made, the work is that of my alone; the work has not been submitted previously, in whole or in the part, to qualify for any other academic award; the content of the thesis is the result of work which has been carried out since the official commencement date of the approved research program; and, any editorial work, paid or unpaid, carried out by a third party is acknowledged.

Umer Javeed

112–FET/MSEE/F07

Abstract

Blind image deconvolution is a very challenging and important research field. It has been proven to be useful in many application areas such as medical imaging, astronomical imaging and remote sensing. Several methods have been used for single channel framework, but in this thesis Multichannel blind deconvolution problem has been proposed when the original image is assumed to be sparse and limited knowledge of the point spread function is available. The sparse nature of image has leaded us to consider the case of Magnetic Resonance Force Microscopy (MRFM), hence PSF of MRFM machine is used in this project. An alternating minimization algorithm is used for the purpose of restoring the original image. The proposed approach has successfully restored the original image and system's PSF.

Acknowledgement

This thesis and all my incessant efforts are of worth only by grace of Allah Almighty, the Exalted, the Most Merciful and the Beneficial Who gave me strength beyond my capabilities to complete this task to the best of my knowledge and abilities.

I would express my gratitude to **Dr. Tanweer Ahmad Cheema**, my respected teacher and supervisor, who cooperated, guided and facilitated us a lot during my thesis. Without his sincere and cooperative nature, I could never have been able to complete this task. I would also like to thank my respected teacher **Dr. Ijaz Mansoor Qureshi** who always been a source of inspiration during my MS studies. My appreciation also goes to **Dr. Aqdas Naveed** for all his support during my thesis.

I would also express my gratitude to my loving parents, without their support and help I would never had been able to accomplish this task. I am also thankful to my friends who helped me a lot during my thesis.

TABLE OF CONTENTS

CHAPTER 3

BLIND IMAGE DECONVOLUTION **12**

CHAPTER 4

CHAPTER 5

CHAPTER 6

List of Figures

List of Tables

CHAPTER 1

INTRODUCTION

Blind image deconvolution is an important and difficult task in image processing. The goal of blind deconvolution is to restore the original image that has been degraded by system and atmospheric noise. Most restoration techniques assume that the system response is already known, but in case of blind image deconvolution, the system response is not known apriori hence it increases the difficulty of restoration task.

1.1   Problem Statement

Multichannel techniques are utilized in the cases where we need to store the multiple images of the same sample. Each image of the sample is acquired through imaging machine and is passed through a channel. The channel contains its Point Spread Function (PSF), when acquired image passes through a channel this leads to convolution between PSF and the acquired image, this results in blurring of the image. Each channel is also prone to atmospheric noise, which is usually regarded as additive Gaussian noise with zero mean. Hence the image acquisition process results in a

blurred and noisy image of the sample and we get a degraded version of the input image.

The application where multichannel image acquisition is applied includes astronomical imaging, satellite imaging and most important of all in the microscopic imaging [1]. This has lead us to focus towards the relatively new imaging technology which is considered as a non-destructive method through which 3-Dimensional images of sub surface properties of a broad range of materials could be obtained with atomic resolution. Image acquisition at atomic level introduces a feature known as sparseness [2]. At such a high resolution most of the image would be comprised of empty space and only a few pixel locations will be containing atoms.

The thesis proposes a multichannel blind image deconvolution method which uses Alternating Minimization Algorithm. The results are subjected to sparseness and smoothness constraints.

1.2 Outline of Thesis

Chapter 2 provides an overview of the Magnetic Resonance Force Microscopy (MRFM) machine which is used as a tool for imaging molecular data. Its comparison with other existing techniques is carried out. Design and basic operating principle of MRFM machine and construction of the Point Spread Function are discussed.

Chapter 3 explains the image restoration problem using blind image deconvolution, image formation model is discussed. Review of existing approaches is presented for the problem of single channel and multichannel blind image deconvolution.

Chapter 4 describes the working of Alternating Minimization Algorithm for the purpose of blind image deconvolution, assumptions and imposed constraints are explained. A proposed method has been presented in order to extend the use of A.M Algorithm for multichannel blind image deconvolution problem.

Chapter 5 contains the results obtained by simulating the proposed method, error graphs have been generated, and convergence issues of the algorithm have been discussed. Evaluation of the algorithm has been conducted on the basis of MSE, NMSE, SNR and ISNR under controlled environment.

Chapter 6 contains the conclusion and future directions.

CHAPTER 2

MAGNETIC RESONANCE FORCE MICROSCOPY

In the early 1990's, the invention and initial demonstration of Magnetic Resonance Force Microscopy (MRFM) initiated a series of mechanical approaches in order to detect magnetic resonance. MRFM is considered as a non-destructive method through which 3-Dimensional images of sub surface properties of a broad range of materials could be obtained with atomic resolution. MRFM differs from the existing technologies in both image resolution and operating principle, which we will discuss in this chapter.

2.1   MRFM difference with existing approaches

All these advancements in medical imaging capabilities have brought revolution in the field of medical diagnostics. This would have not been possible without the use of sophisticated imaging algorithms which were used during the image acquisition and observing the areas of interest. Some of these techniques are discussed below, along with their positive as well as negative features.

2.1.1 Electron microscopes

An electronic microscope uses high intensity particle beam of electrons in order to illuminate the specimen, which results in a highly magnified image. Electro-magnetic and electrostatic lenses are used in this microscope for the formation of image by controlling the beam in such a way that the beam can be focused at a specific plane in accordance with the sample. Since this technique uses the wavelength of an electron, hence the achievable resolution is up to 2 million times.

The disadvantages of using this technique for imaging are that high intensity electron beams disrupts the fragile molecules in delicate biological structures, in order to operate they also require highly stable high voltage supplies and stable currents for each electromagnetic lens.

2.1.2 X-ray crystallography

This imaging technique uses a method of determining the arrangements of atoms within a crystal, a beam of X-rays strikes on a crystal and scatters into many different directions. By using the intensities and angles of these diffracted beams, they crystallographer produces a 3-Dimensional image of the electron density inside the crystal.

This technique has been used excessively in the field of bio-medical engineering for analyzing the structures of various proteins. The main challenge for the crystallographers remains to coax the biological molecules in such a way that they form ordered solids which are amenable to X-ray analysis. Majority of the proteins are not suitable to be analyzed by X-ray crystallography is because they are not

capable to form crystals; hence many important protein topologies are poorly suited to X-ray analysis.

2.1.3 Nuclear Magnetic Resonance

NMR spectroscopy is a technique which exploits the magnetic properties of the nuclei. It is used to obtain physical, chemical as well as structural information of the molecules. Despite other approaches, as described above, Nuclear Magnetic Resonance is also used for the analysis of proteins.

It uses sophisticated and complex techniques for manipulating the spin behavior, but it applies restrictions on the protein samples which need to be studied. It requires expressible proteins which are soluble in milli-molar concentrations but it does not scale to large molecules or their combinations.

2.1.4 Atomic Force Microscopy

The atomic force microscope (AFM) is a very high resolution microscope which belongs to the class of scanning probe microscopy. Its demonstrated resolution approaches to fractions of a nanometer (10^{-9}). AFM is an advanced type of Scanning Tunneling Microscope (STM) and is mostly used for measuring and imaging a sample in nano scale resolution.

The AFM consists of a micro-scale cantilever with a sharp tip at its end, which is used to scan the sample surface. When the tip gets closer to the surface of the sample, deflections is caused in the cantilever because of the magnetic field on the tip and the magnetic field of the sample. This deflection is measured with the help of a laser light pointing at the surface of cantilever, when cantilever is deflected by magnetic fields,

-6-

this laser beam is reflected from the surface in to light detectors which are capable of recording any minute deflection. This principle can provided higher resolution as compare to which we have already achieved by using other techniques, and it has been shown to give atomic resolution in high vacuum environment [3].

AFM has many advantages over the electron microscope. The electron microscope needed an ideal vacuum environment for effective operation whereas AFM can work perfectly well inside liquid environment, which makes the study of biological macro-molecules possible.

The disadvantage of AFM is that if the tip is not selected correctly for the deflection measurement then it can lead to image artifacts. AFM also scans the images slowly as compare to electron microscope. Due to nature of AFM experiment, it is limited to surface imaging only.

2.1.5 Magnetic Resonance Imaging

Magnetic Resonance Imaging (MRI) is another medical imaging technique which is mostly used in radiology in order to visualize the internal structure of the body and provides us the three dimensional Imaging capability. It provides much greater contrast between the different soft tissues of the body than any other existing technique. Because of this property it is extensively used for diagnosing infections in the brain, spinal cord and joints, as well as for visualizing tumors, torn ligaments and shoulder injuries. MRI is currently limited to dimensions greater than tens or even hundreds of micrometers due to poor sensitivity of the inductive technique of magnetic resonance detection [4].

Till now the applications and limitations of all the major imaging techniques have been discussed which are being used for high resolution viewing of atoms and molecular structures. The MRFM detects atomic and sub-atomic forces mechanically, whereas MRI detects small electrical signals. MRFM is a novel scanned probe instrument that has combined the key features of Atomic Force Microscopy (AFM), i.e. its high resolution imaging capability and high sensitivity, with the 3-Dimensional imaging capabilities of Magnetic Resonance Imaging (MRI) [5]. MRFM offers the possibility of shrinking the sample size into sub-micrometer level, with the clear possibility of achieving atomic scale resolution. It is likely that the MRFM will ultimately match the resolution achievable in scanning probe microscopes such as electron microscopes and atomic force microscopes.

2.2   The Features of MRFM

Microscopic MRFM studies will be helpful in providing us the knowledge about the physics of magnetic and other materials. The salient feature of an atomic level imaging system is its sparse nature. At such a high resolution most of the image would be empty space, and only a few spatial locations would contain the molecules.

2.2.1 MRFM Experiment

Strong field gradients are used in MRFM in order to create such environment in which NMR pulse can be interpreted. The fundamental feature of an MRFM experiment is the mechanical microscopic cantilever. This is like holding two bar magnets and feeling the polar forces without actually touching them together. At a few atto-newtons (10^{-18}) the force exerted by an electron spin on an MRFM cantilever is a million times weaker than the forces encountered in an atomic force microscopy

[6]. The spin's magnetic orientation flips back and forth as the cantilever vibrates. The flipping of the spin causes a detectable change in the cantilever's vibration frequency.

The detailed experiment model has been shown in figure 2.1, which shows the sample container where sample is to be placed, Fiber optic inferometer is used to detect any minute displacement occurred in cantilever's position. Tip of the cantilever contains tiny particles of ferro magnet, which helps in producing deflection and increases the sensitivity of the MRFM tip. RF coil is used to achieve resonance frequency of the sample, such that it creates enough force to cause a deflection of the cantilever.
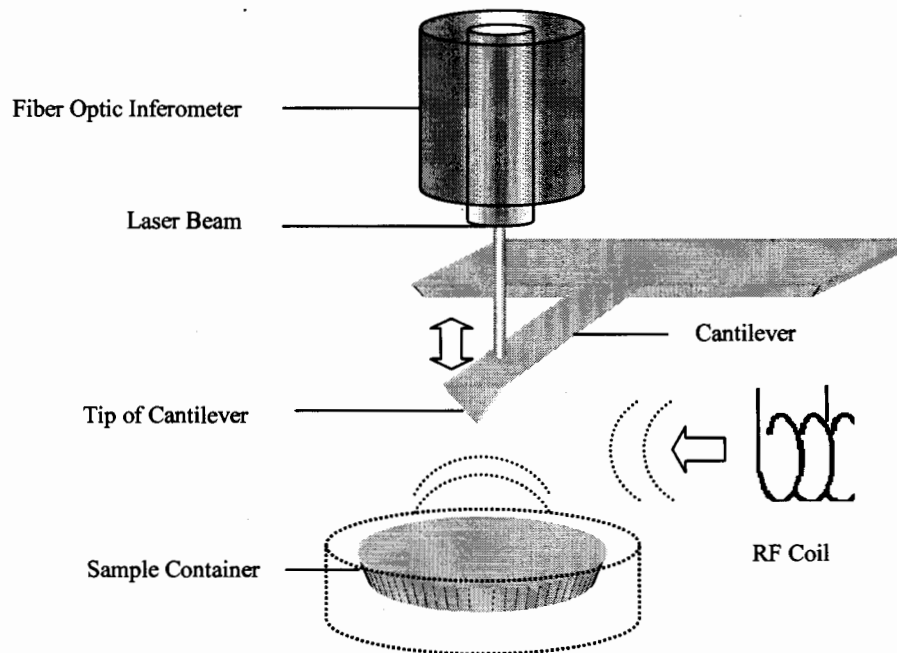
Figure 2. 1: Configuration of single spin MRFM Experiment

The results of MRFM mostly improve with sharper and smaller cantilevers. Hence it directly relates to the sensitivity measure in the signal to noise ratio (SNR), but design tradeoffs emerge at the standard quantum limit. A stiffer cantilever, for example, offers better control over noise but requires a stronger signal to move it. Likewise,

softer, lighter cantilevers are capable of sensitive detection but ate buffeted by the process and measurement noise.

Current experiments are conducted in a vacuum of around 10^{-5} torr. As the cantilever scans over the surface of the sample, recording the MRFM signal, the distribution of spins of the sample can be reconstructed. The IBM researchers detected the signal of a single electron spin using interrupted OSCAR protocol.

2.2.2 Point Spread Function

The signal processing involved in measuring the PSF of the MRFM machine has been derived in [7] based on the parameters given in [8]. The PSF is considered to base upon the parameters like external magnetic field, magnetic field of the resonance slice and cantilever tip movement. In Table 2.1 a list of parameters is given which forms the PSF.

Table 2.2: Parameters used for MRFM's PSF

Description	Name	Value
External magnetic field's amplitude	B_{ext}	2×10^4 G
B_{mag} in the resonant slice	B_{res}	2.24×10^4 G
Radius of tip when modeled as sphere	R_0	2nm
Distance from tip to sample	d	2nm
Cantilever tip movement	m	5.70×10^4 emu
Peak cantilever swing	x_{pk}	0.033nm
Maximum magnetic field gradient	G_{max}	610 G/nm

The original PSF has been shown in [7], whereas certain idealized form of MRFM's PSF has been used in [9] [10]. The idealized 2-Dimension PSF form which is being

used in the thesis is given in figure 2.1, in which it is assumed that the cantilever used in MRFM experiment is an ideal cylindrical spindle.
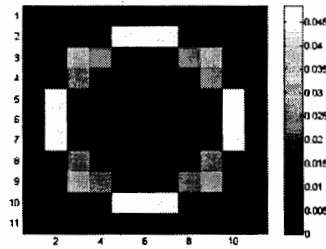
Figure 2.2: MRFM Point Spread Function

The point spread function of MRFM, shown in figure 2.2 will be used for simulations. The properties and features of this point spread function are discussed in detail under topic 3.1.1. In this thesis with the help of Alternating Minimization algorithm not only the original sent image will be retrieved out of multiple observations but also its point spread function will be reconstructed.

CHAPTER 3

BLIND IMAGE DECONVOLUTION

The image deconvolution has been widely studied in the literature due to its importance in many application fields such as astronomy, microscopy, medical imaging and distant imaging. The problem of image deconvolution is the process of recovering the original image from a single or multiple degraded observations. The approaches which can be used for the purpose of deconvolution depend not only on the image degradation model but also on the degraded observation of the input image.
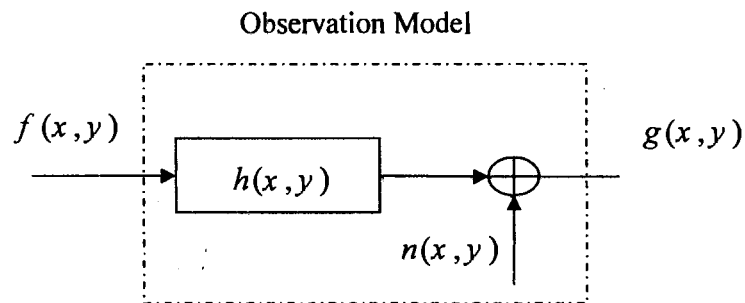
Observation Model

Figure 3.1: Linear space invariant image degradation model

A linear degradation model is commonly employed in many applications. In this model, the observed image is a result of convolution between original image and a point spread function (PSF) in the presence of additive white Gaussian noise. In order to retrieve the original image out of the blurred and noisy observation the estimation of blur filter is required in the classical image deconvolution techniques. However, in many practical situations, the PSF is either partially known or completely unknown. Therefore, the PSF needs to be estimated from the degraded image observation and such methods are known as blind image deconvolution methods.

Classical image restoration seeks an estimate of the true imaging assuming the blur is known, where as blind image restoration handles much more difficult yet realistic problem, where the degradation is unknown [11]. In general, the degradation is nonlinear and spatially varying process. However, for most of the work, it is assumed that the observed image is the output of a Linear Spatially Invariant (LSI) system to which noise is added. If the Point Spread Function is not known apriori then the problem becomes a Blind Deconvolution (BD) problem.

3.1 Mathematical Formulation

In digital image processing, the general discrete model for a linear degradation caused by blurring and additive noise is given by

$$g(x,y) = h(x,y) * f(x,y) + n(x,y) \qquad (3.1)$$

Where $f(x,y)$ represents an original $M \times N$ image, and $g(x,y)$ is the degraded image which has been acquired by the imaging system. In the above equation $n(x,y)$ represents an additive noise introduced by the system, and is taken as zero mean,

Gaussian distributed white noise. This results to the following expression for the degrading system.

$$g(x,y) = \sum_{k=1}^{M}\sum_{l=1}^{N} h(x-k,y-l)f(k,l) + n(x,y) \qquad (3.2)$$

Where * indicates two dimensional convolution, $f(x,y)$ is of size $M \times N$, $h(x,y)$ is a matrix of size $J \times K$, and $g(x,y)$ is therefore of size $(M+J-1)\times(N+K-1)$, similarly $n(x,y)$ is also of size $(M+J-1)\times(N+K-1)$.

Since the space variant degradations results into very complex solutions, we have used the shift invariant model so that linear techniques can be applied on them. This above mentioned model formation can also be represented in Matrix-vector form.

$$g = Hf + n \qquad (3.3)$$

H is a Block Toeplitz with Toeplitz Blocks (BTTB) matrix and can be approximated by a Block Circulant with Circulant Blocks (BCCB) matrix. Since BCCB matrices can be diagonalized using the 2-D Discrete Fourier Transform (DFT) [12], this allows us to work on it in frequency domain.

Here the vectors g, f and n represent the observed image, the original image, and the observation noise. Lexicographically by stacking the rows of each image into a vector, the f becomes vector of size $MN \times 1$, the blurring matrix H becomes matrix of size $(J+M-1)(K+N-1)\times MN$, and the noise n becomes a vector of length $(J+M-1)(K+N-1)\times 1$, similarly the observation vector g is of length $(J+M-1)(K+N-1)\times 1$. The **H** matrix is defined as,

$$\mathbf{H} \square \begin{bmatrix} [\mathbf{H}_1] & \cdots & & & 0 \\ \vdots & \ddots & & & \vdots \\ [\mathbf{H}_J] & & \ddots & & [\mathbf{H}_1] \\ \vdots & & & \ddots & \vdots \\ 0 & & \cdots & & [\mathbf{H}_J] \end{bmatrix} \tag{3.5}$$

In order to understand the structure in better way, the entire model given in equation 3.3 can also be redefined for a single row of observation g as,

$$g_1 = [\mathbf{H}_1] f_1 \tag{3.6}$$

The equation 3.6 can also be written in element wise form as,

$$\begin{pmatrix} g(1,1) \\ g(1,2) \\ \vdots \\ \vdots \\ g(1,K+N) \end{pmatrix} = \begin{bmatrix} h(1,1) & \cdots & & & 0 \\ \vdots & \ddots & & & \vdots \\ h(1,K) & & \ddots & & h(1,1) \\ \vdots & & & \ddots & \vdots \\ 0 & & \cdots & & h(1,K) \end{bmatrix} \begin{pmatrix} f(1,1) \\ f(1,2) \\ \vdots \\ \vdots \\ f(1,K+N) \end{pmatrix} \tag{3.7}$$

Now this illustration shall help us in order to understand that how does it work for the entire image formation,

$$\begin{pmatrix} g_1 \\ g_2 \\ . \\ . \\ g_{J+M} \end{pmatrix} = \begin{bmatrix} [\mathbf{H}_1] & \cdots & & & 0 \\ \vdots & \ddots & & & \vdots \\ [\mathbf{H}_J] & & \ddots & & [\mathbf{H}_1] \\ \vdots & & & \ddots & \vdots \\ 0 & & \cdots & & [\mathbf{H}_J] \end{bmatrix} \begin{pmatrix} f_1 \\ f_2 \\ . \\ . \\ f_M \end{pmatrix} \tag{3.8}$$

After performing this operation we will get a vector 'g' of size $(J+M-1)\times(K+N-1)$. Blind deconvolution problem refers to finding estimates $\hat{f}(x)$ and $\hat{h}(x)$ for $f(x)$ and $h(x)$ based on $g(x)$ and any available prior knowledge about $f(x)$, $h(x)$ and $n(x)$.

3.1.1 Properties of H

1) We know that generally blurred observation occurs as a result of the convolution between the original image '$f(x,y)$' and the point spread function '$h(x,y)$', in such a situation, $f(x,y)$ and $h(x,y)$ are matrices of dimension $M \times N$ and $J \times K$ respectively. But when we transform this convolution matrices problem into a matrix-vector form, we get the transformed 'f' and 'H' of dimensions $MN \times 1$ and $(J + M - 1)(K + N - 1) \times MN$ respectively [13]. Structure of matrix H can be seen in equation (3.5).

The results produced from convolving '$h(x,y) * f(x,y)$' are same as that of multiplication of 'Hf', when H describes a convolution its Toeplitz and if it is zero padded in an appropriate way, it results in a Circulant matrix.

2) Since the linear operator H acting on vector 'f' is considered to be the convolution operator, by the commutative property of convolution, it may also be written as $Hf = Fh$. It means that equation (3.3) can also be written as

$$g = Fh + n \tag{3.9}$$

In order to prove this equality we need to transform the vector 'f' into a Circulant matrix F the way it was done before with H, which can be seen in equation (4.5).

3) F is assumed to be a Circulant matrix and hence diagonalizable by the DFT matrix [14], which is denoted by D. Thus we write

$$\mathbf{F} = \mathbf{D}diag\,(\mathbf{D}^H f\,)\mathbf{D}^H$$

$$\mathbf{H} = \mathbf{D}diag\,(\mathbf{D}^H h)\mathbf{D}^H$$

$$\Delta = \mathbf{D}diag\,(\mathbf{D}^H \delta)\mathbf{D}^H \tag{3.10}$$

Here $diag\,(\mathbf{x})$ represents a diagonal matrix whose entries are the elements of $\mathbf{x}$. This treatment is amenable to analysis and yields computational savings, as matrix multiplication becomes convolution, which may be efficiently implemented via the FFT [15].

3.2 Review of Blind Deconvolution Techniques

Observing the Image formulation model, the difference of restored image and original image can be represented by the following cost function,

$$J(f) = \left\|\mathbf{H}f - g\right\|^2 \tag{3.11}$$

Here a brief introduction has been given to the techniques which are being used for the process of Blind Image Deconvolution.

3.2.1 Inverse filter

In the inverse filter, the objective function mentioned in equation (3.11) needs to be dealt with. While analyzing the objective function it can be observed that such $\hat{f}$ should be found which minimizes the norm of the difference of the restored estimated image $\mathbf{H}\hat{f}$ and the observed image g [16]. In order to minimize this cost function

partial derivate of the equation (3.11) should be taken w.r.t. image f and then setting the equation equal to zero, equation (3.11) results in,

$$\frac{\partial J(f)}{\partial f} = 0 = -2\mathbf{H}^{\mathrm{T}}(g - \mathbf{H}f) \qquad (3.12)$$

And then solving for that f that satisfies the minimum of objective function, the equation results in,

$$\hat{f} = (\mathbf{H}^{\mathrm{T}}\mathbf{H})^{-1} \mathbf{H}^{\mathrm{T}}g \qquad (3.13)$$

Hence the inverse filter will become,

$$Inverse\,filter = (\mathbf{H}^{\mathrm{T}}\mathbf{H})^{-1} \mathbf{H}^{\mathrm{T}}g \qquad (3.14)$$

The problem with this method is that if our point spread function $\mathbf{H}$ is singular then $\mathbf{H}^{\mathrm{T}}\mathbf{H}$ will also result in singular and hence their inverse cannot be calculated. This way the technique will not remain applicable.

3.2.2 Constrained Least Square Filter

In order to make the filter more effective, rather than just doing inversions, such constrained least squares filter is needed to be developed in which the constraint provides additional control over the restoration process [17]. For this purpose we minimize the objective function $J(f)$ with subject to a constraint on image 'f' that the image can only take 'p' number of non-zero values. This way the cost function will have to be minimized, keeping in view the applied constraint and the cost function will become of the form,

$$J(f) = \min_{f} \|Hf - g\|^2 \; such that \; \|f\|_1 \le p \tag{3.15}$$

$$J(f) = \|Hf - g\|^2 + \lambda \|f\|_1 \tag{3.16}$$

In order to minimize this cost function, partially derivate should be applied on the image 'f'.

$$\frac{\partial J}{\partial f} = 0 = 2H^T(Hf - g) + 2\lambda(f) \tag{3.17}$$

$$H^T g = H^T H f + \lambda f$$

$$H^T g = (H^T H + \lambda I)f \tag{3.18}$$

Now solving for the f that provides the minimum of the objective function yields

$$\hat{f} = \left[(H^T H + \lambda I)^{-1} \right] H^T g \tag{3.19}$$

$$Constrained \; Least \; Square \; Filter = \left[(H^T H + \lambda I)^{-1} \right] H^T \tag{3.20}$$

The Lagrangian 'λ' must be adjusted such that the constraint can be satisfied. This is mostly done in an iterative manner.

3.2.3 Parametric Wiener Filter

The wiener filter is considered optimum keeping in view the mean square error. This filter is designed by minimizing the mean square error between the restored image and the original image.

$$J(f) = \left\| \Phi_{ff}^{-1/2} \Phi_{nn}^{1/2} f \right\|^2 + \|Hf - g\|^2 \tag{3.21}$$

Now in order to minimize the cost function the partial derivative will be applied, which results in

$$\frac{\partial J}{\partial f} = 2\left(\Phi_{ff}^{-1/2}\Phi_{nn}^{1/2}\right)^{T}\left(\Phi_{ff}^{-1/2}\Phi_{nn}^{1/2}\right)f - 2H^{T}\left(Hf - g\right) = 0 \tag{3.22}$$

Solving the equation for the estimated $\hat{f}$,

$$\hat{f} = \left[H^{T}H + \Phi_{ff}^{-1}\Phi_{nn}^{1}\right]^{-1}H^{T}g \tag{3.23}$$

Hence the Wiener filter becomes,

$$Wiener\ filter = \left[H^{T}H + \Phi_{ff}^{-1}\Phi_{nn}^{1}\right]^{-1}H^{T} \tag{3.24}$$

where $\Phi_{ff} = E(ff^{T})$ and $\Phi_{nn} = E(nn^{T})$ represents the covariance matrices of original image f and the noise n respectively. Wiener filter is derived optimally but its success depends on how accurate are the estimates of original image and noise matrices. In practical situations, one is provided with degraded observation g and it is needed to approximate Φ_{ff} out of Φ_{gg}. The variance of the noise is assumed to be known and is also assumed that noise n is uncorrelated with the original image f.

If current objective function is replaced with the one which was used for "Constrained Least Squares filter" and carrying all the derivations on it, then "Parametric Wiener Filter" can be defined as,

$$Parametric\ Wiener\ Filter = \left[H^{T}H + \lambda\Phi_{ff}^{-1}\Phi_{nn}^{1}\right]^{-1}H^{T} \tag{3.25}$$

3.2.4 Iterative Blind Deconvolution Algorithm

This method is one of the most popular methods which are being utilized for the deconvolution purpose. Other than the main features, non-negativity and finite support, its approach is similar to Wiener filter's constraints in order to estimate the original image and Point Spread Function in Fourier domain. The fundamental structure of the algorithm is shown in Fig 3.2.
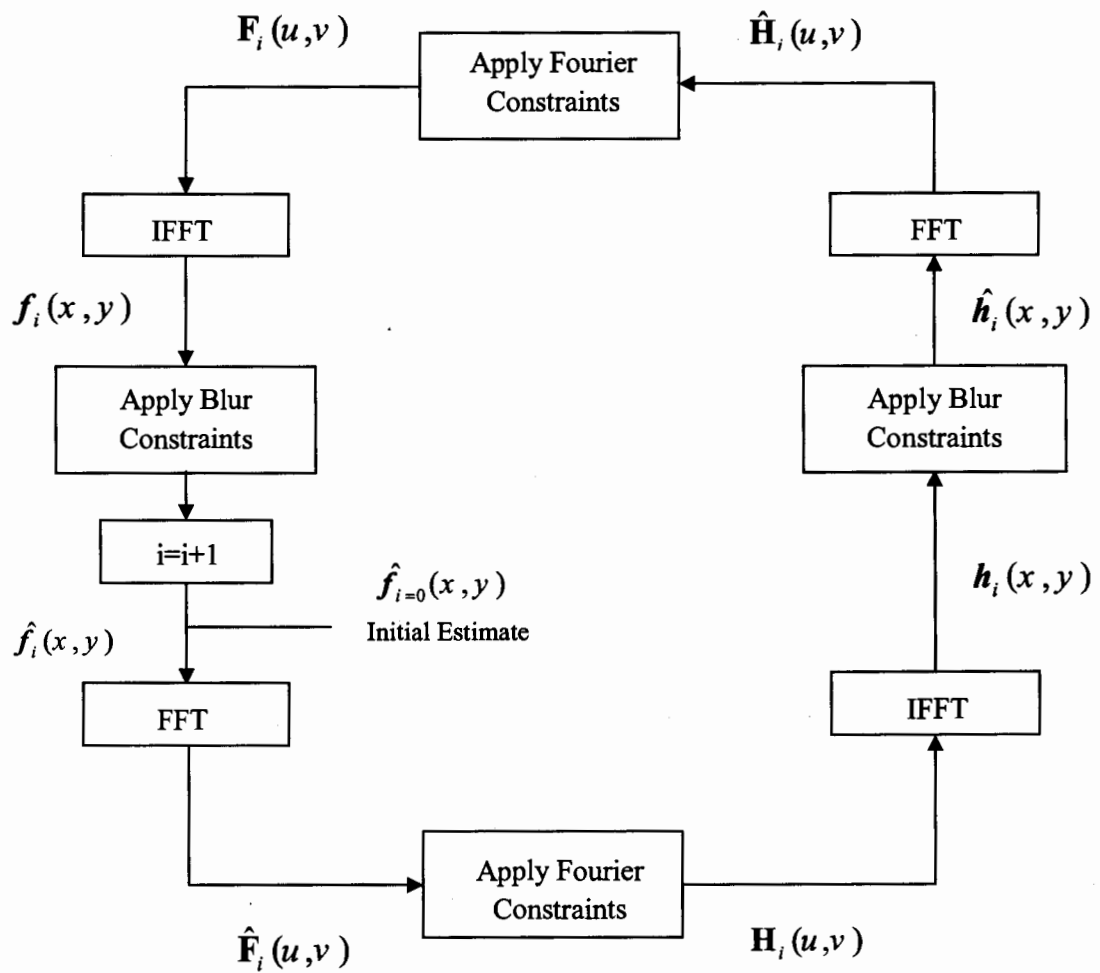
Figure 3.2: Iterative blind deconvolution algorithm model

The initial estimate is denoted by $\hat{f}_{i=0}(x,y)$, the PSF estimate by $\hat{h}_i(x,y)$, and the linearly degraded image by $g(x,y)$. $\mathbf{F}_i(u,v)$ and $\mathbf{H}_i(u,v)$ represents the Fast Fourier Transform (FFT) of $f_i(x,y)$ and $h_i(x,y)$ respectively, whereas their sub script 'i' denotes the iteration number.

After the initialization for the image, the algorithm keeps on alternating between the image and the Fourier domains meanwhile enforcing the constraints. The constraints are applied on the basis of information available regarding the original image as well as the PSF.

The algorithm starts working with given estimate of the original image $f(x,y)$ i.e. $\hat{f}_{i=0}(x,y)$, on taking its FFT and imposing the Fourier constraint we are able to extract $\mathbf{H}_i(u,v)$ out of $\hat{\mathbf{F}}_i(u,v)$ which can also be seen through equation (3.22). Now the inverse FFT of $\mathbf{H}_i(u,v)$ is taken, which results in $h_i(\dot{x},y)$ and after imposing the blur constraint on the PSF estimated $\hat{h}_i(x,y)$ is achieved. When FFT is applied on it then $\hat{\mathbf{H}}_i(u,v)$ is achieved. On applying the Fourier constraints on $\hat{\mathbf{H}}_i(u,v)$, the $\mathbf{F}_i(u,v)$ is produced, also explained in equation (3.23) and if Inverse FFT is applied on it, then it is transformed back into the time domain i.e. $f_i(x,y)$.

The image $f(x,y)$ and PSF $h(x,y)$ are both assumed to be non-negative with finite known support. In order to implement these constraints, the pixels within the region of support having negative values and nonzero pixels outside the region of support are replaced with the zero valued pixels [18]. In the Fourier domain

constraint, the PSF is estimated by using the FFT of estimated PSF and the degraded blurred and noisy observation. Hence at the nth iteration we have

$$\mathbf{H}_n(u,v) = \frac{G(u,v)\hat{\mathbf{F}}_{n-1}^T(u,v)}{\left|\hat{\mathbf{F}}_{n-1}(u,v)\right|^2 + \alpha / \left|\mathbf{H}_{n-1}(u,v)\right|^2} \tag{3.26}$$

$$\mathbf{F}_n(u,v) = \frac{G(u,v)\hat{\mathbf{H}}_{n-1}^T(u,v)}{\left|\hat{\mathbf{H}}_{n-1}(u,v)\right|^2 + \alpha / \left|\mathbf{F}_{n-1}(u,v)\right|^2} \tag{3.27}$$

The 'α' alpha denotes the energy of noise, it should be chosen carefully for good restoration. This method is majorly used because of low complexity. The major disadvantage of the method is its lack of reliability and the restoration is sensitive to the initial image estimate.

3.2.5 Bayesian Method

The Bayesian methodology has been widely used for the Blind Image Deconvolution problem [16]. The algorithms which are based on Bayes Law differentiate from other algorithms since these algorithms include the prior knowledge about the original image f in the form of a prior probability distribution over images.

In order to deal with the problem of image deconvolution in algorithms, which comprises of Bayes Law, the first thing which is required, is to evaluate the probability density function of original image f i.e. $p(f)$.

Here it is assumed that the probability density function $p(f)$ carries high probability to such solutions which matches with the prior knowledge. The prior knowledge has been assumed about the original image and the prior distribution is also constructed

independent of the blurred and noisy observation g. The Bayes Law comprises of the conditional probability density relationship

$$p(f \, / \, g) = \frac{p(g \, / f) p(f)}{p(g)} \tag{3.28}$$

Now in order to maximize the probability $p(f \, / \, g)$ the right hand side of the equation will have to be maximized. On the RHS $p(g)$ cannot be maximize since its probability if received degraded observation and hence its value is fixed. Similarly the probability of original image i.e. $p(f)$ also cannot be maximized, so $p(g \, / f)$ will have to be maximized [19].

3.2.6 Maximum Likelihood (MLL) Methods

The application of the method of Maximum Likelihood approximation in the problem of image deconvolution comprises of the random properties of observed image g, which are already known [20]. If the Point Spread Function (PSF) is already known, then the probability density function $p(g \, / f)$ is only a function of original image f, hence our deconvolution problem shrinks up to the estimation of the unknown parameters of the original image f.

The Maximum Likelihood estimate is the original image f which will most probably produces the observed blurred and noisy image g. In order to avoid mathematical complexities it is preferable to use log-likelihood function, the Maximum likelihood solution is found by solving the equation,

$$MLL \; Estimate = \max p(g \, / f)$$

3.2.6.1 Maximum Likelihood with Gaussian PDF Noise

Since it has already been discussed that the probability $p(g / f)$ is needed to be maximized, if the added noise if of Gaussian PDF then the equation will become,

$$p(g / f) = \frac{1}{\sqrt{2\pi\sigma^2}} \exp\left(-\frac{\|g - Hf\|^2}{2\sigma^2}\right) \qquad (3.29)$$

Here 'σ^2' denotes the variance of the noise, since $p(f)$ is a constant therefore in order to maximize $p(f / g)$ is needed to be minimized.

$$J(f) = \frac{\|g - Hf\|^2}{2\sigma^2} \qquad (3.30)$$

The denominator part is a constant and will not play any role in minimization the equation, hence the minimization of equation can be achieved using iterative techniques such as steepest descent method. The solution is found by iteratively updating the equation,

$$f^{n+1} = f^n + \lambda H^T\left(g - Hf^n\right) \qquad (3.31)$$

Where H^T denotes the transpose of PSF, f^n represents the current desired estimate of original image and f^{n+1} represents the updated estimate of original image. This method is usually refer to as 'Landweber iteration' [21], furthermore certain conditions like de-noising or non negativity can also be applied on each iteration, and when the stopping criterion is met then iterations can be stopped.

3.2.6.2   Maximum Likelihood with Poisson PDF Noise

This case is different from the previous discussed Gaussian case, since the noise which is being added is of Poisson distribution. Similarly the probability $p(g/f)$ will also not remain same rather it will become

$$p(g/f) = \prod_{x,y} \frac{H(x,y)f(x,y)g(x,y)\exp\{-H(x,y)f(x,y)\}}{g(x,y)!} \quad (3.32)$$

Since the probability of $p(g/f)$ is needed to be maximized, hence partial derivate is applied on the equation (3.30) by original image i.e. $f(x,y)$

$$\frac{\partial \ln p\{g(x,y)/f(x,y)\}}{\partial f(x,y)} = 0 \quad (3.33)$$

Upon solving the equation and assuming the PSF is normalized to unity, the equation results in,

$$\left[\frac{g(x,y)}{H(x,y)f(x,y)}\right]H^{T}(x,y) = 1 \quad (3.34)$$

Multiplying both sides by $f(x,y)$, the equation becomes

$$f(x,y) = \left[\frac{g(x,y)}{H(x,y)f(x,y)}\right]H^{T}(x,y)f(x,y) \quad (3.35)$$

By applying the Picard iteration [22] on equation (3.33), it becomes

$$f^{n+1}(x,y) = \left[\frac{g(x,y)}{H(x,y)f^{n}(x,y)}\right]H^{T}(x,y)f^{n}(x,y) \quad (3.36)$$

Where 'n' denotes the iteration number and $\mathbf{H}^{\mathrm{T}}$ denotes the transpose of the PSF. This is commonly known as 'Richardson-Lucy algorithm' [20]. The Richardson-Lucy algorithm is mostly used in astronomical problems, since it preserves the total intensity and the solution is always positive. This algorithm is constrained but non-regularized and hence provided that the initial estimate for the image *f(0)* is non-negative then *f(n)* will remain non negative.

3.2.7 Maximum a Posteriori (MAP) Method

M.A.P method utilizes the regularization approach [23]. This can be achieved by using an appropriate prior probability density function $p(f)$. This $p(f)$ can be considered as a constraint function which prevents the undesired features of the solution, in accordance with the general observation of the original image f. The maximization of the constrained likelihood can be seen as the maximization of the posteriori probability.

$$\hat{f} = \arg\min p(g/f)p(f) \tag{3.37}$$

Now the case of Maximizing a Posteriori Probability will be considered when the added noise is of Poisson probability density function. The PDF of original image 'f' can be written as,

$$p(f) = \prod_{x,y} \frac{A(x,y)f(x,y)\exp\{-A(x,y)\}}{f(x,y)!} \tag{3.38}$$

Using the derivation, the Maximum a Posteriori solution results in,

$$f(x,y) = A(x,y) \exp\left\{ \left[\frac{g(x,y)}{\mathbf{H}(x,y)f(x,y)} - 1 \right] \mathbf{H}^{\mathrm{T}}(x,y) \right\} \qquad (3.39)$$

Now estimating $A(x,y) = f^n(x,y)$ and using the Picard iteration, the equation becomes,

$$f^{n+1}(x,y) = f^n(x,y) \exp\left\{ \left[\frac{g(x,y)}{\mathbf{H}(x,y)f^n(x,y)} - 1 \right] \mathbf{H}^{\mathrm{T}}(x,y) \right\} \qquad (3.40)$$

3.3 Multichannel Blind Image Deconvolution

Up till so far the Blind Image Deconvolution problem has been discussed, when the acquired image passes through a channel and white Gaussian noise is being added in it, this kind of restoration is known as Single Channel Blind Image Deconvolution. In some applications the image acquiring system is able to give multiple observations of the original image. Hence several blurred versions of the same original image are received which are being observed through different acquisition channels.

In electron microscopy, multiple images are acquired of the same sample by altering the focus of the system during a single experiment. In remote sensing systems, the same scene can be acquired on different time slots through the atmosphere by using the sensor diversity, such channel can be modeled as a time-variant channel. While in other applications, for example, Tele-surveillance, multiple images are acquired in order to deal with the possible degradations in a better way, which may get produced because of de-focusing, atmospheric noise or degradation due to motion [24] [25].

When these channels are frequency bands, such problem is referred as multi-spectral images, if the same scene is captured at different time slots, they are known as image sequences. If different observations of the same image are acquired by using different channels then we can treat this scenario as multichannel representation and restoring the original image through these multiple degraded observations without knowing the channel response is known as Multichannel Blind Image Deconvolution.

3.3.1 Mathematical Formulation

Now the model will not remain a simple linear model, rather we will have to consider the Single Input Multiple Output scenario (SIMO), where a single image is captured by a same source (MRFM) at different instants of time or at different focus, at the end multiple copies of same image will be received passing through different channels which causes varying noise levels and varying system response functions. Such problem can be mathematically represented as,

$$g_i(x,y) = h_i(x,y) * f(x,y) + n_i(x,y)$$

$$g_i(x,y) = \sum_{k=1}^{M} \sum_{l=1}^{N} h_i(x-k,y-l) f(k,l) + n_i(x,y) \quad (3.41)$$

Let J be the number of channels $h_i(u,v)$, $i = 1,2......J$ each of size $M \times N$, hence by stacking the J vectors g_i into a single vector we get,

$$g(x,y) = [g_1^T(x,y), g_2^T(x,y), ... g_J^T(x,y)]^T$$

$$h(x,y) = [h_1(x,y), h_2(x,y), ... h_J(x,y)]^T$$

$$f(x,y) = [f(1,1), f(1,2)....,f(1,N), f(2,1).....f(M,N)]^{\mathrm{T}}$$

$$n(x,y) = [n_1(x,y), n_2(x,y),.............n_J(x,y)]^{\mathrm{T}} \qquad (3.42)$$

It denotes the output images, point spread functions, input image and additive white Gaussian noise respectively.

3.3.2 Methods for MCBID

Many different approaches have been utilized to solve the multichannel blind deconvolution problem; here we will discuss some of them. The Eigen Vector based Algorithm for Multichannel blind deconvolution (EVAM) has been proposed for the deconvolution of an unknown, Gaussian stationary or from two or more unknown channels a non stationary signal is observed. This algorithm is based on Eigen value decomposition of a sample correlation matrix [26]. Multichannel problem has been discussed in which original image is restored out of multiple degraded observations. Results show that both the filters and the image can be determined from degraded observations after applying some assumptions [27]. The Mutually References Equalizers (MRE) method is extended for the case when there is noise in a multichannel framework. Use of regularization procedures has helped in reconstruction of PSF [28]. An alternating minimization procedure is presented which is based on maximum a posteriori estimation with a prior distribution of blurs which are derived from the multichannel framework, whereas a priori distribution of original images is defined by the total variation (TV) semi norm [29]. A novel deterministic framework is applied that allows the image to be non-stationary and have unknown

distribution. The result shows successful blind identification of the blur, blind restoration of original image and also the blind order determination [30]. An algorithm is proposed for direct multichannel blind image restoration considering the case when the noise can be ignored; original images are successfully restored [31]. The general state space approach for the blind deconvolution problem is modified in order to reduce the additional delays; the objective is achieved with the help of balanced parameterization of the discrete-time system [32].

CHAPTER 4

MULTICHANNEL BLIND IMAGE DECONVOLUTION
FOR SPARSE MOLECULAR IMAGING

This chapter introduces the proposed method for restoring the original sparse molecular image out of multiple degraded images acquired through using different channels. It has been discussed in chapter 2 that, the image acquired by using MRFM technique is sparse in nature. Atomic level imaging has sparsity as its salient feature, since only a few spatial locations would be occupied by atoms while most of the image would be empty space. In addition, a smoothing penalty has been used on allowable PSF's to improve the reconstruction.

4.1   Problem definition

Earlier the single channel blind image deconvolution case was discussed, in which the image was acquired through a single channel, AWG noise was being added in it and in the end a blurred and noisy image was observed. By using the blind deconvolution methods we aim to retrieve the original image out of this blurred and noisy

observation, this was regarded as a linear problem, as can be seen by the equation (3.1).

Now the problem is not that simple, now multiple images of the same sample are passing through different channels, each having different PSF and different amount of noise is being added in each observation [33]. In such a situation, original image will have to be deconvoluted out of multiple blurred and noisy observations and will have to select only one estimated $\hat{f}$. This problem can be further explained with the help of figure 4.1.
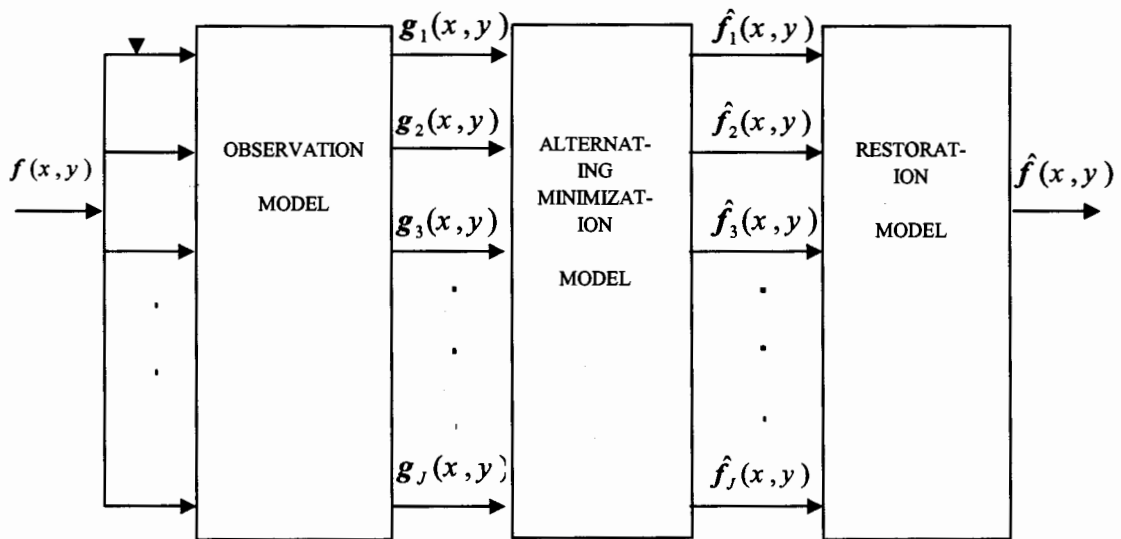
Figure 4.1: Multiplechannel Blind Image Deconvolution Model

4.2   Multichannel Blind Image Deconvolution Model

Observing the figure 4.1, it can be observed that whole Multichannel Blind Image Deconvolution problem can be categorized in to three parts i.e. Observation model, Alternating Minimization model and the last one is Restoration model. The working and the importance of each individual block is discussed below.

4.2.1 Observation Model

The problem of Multichannel Blind Image Deconvolution has been explained here in a better way. The image of the sample is represented by $f(x,y)$, this image passes through 'J' channels, which have PSF's $h_i(x,y)$ and noise $n_i(x,y)$, which causes degradation effects on the original image [34]. After passing though these channels the original image is degraded into blurred and noisy observations which are denoted as $g_i(x,y)$.

$$g_i(x,y) = h_i(x,y)*f(x,y) + n_i(x,y) \tag{4.2}$$

Let J be the number of channels $h_i(x,y)$, $i = 1,2......J$ each of size $M \times N$, details of $g(x,y), h(x,y), f(x,y)$ and $n(x,y)$ vectors has already been discussed in the equation 3.40.

The figure 4.2 explains the working of the observation model, the way it receives the original image $f(x,y)$, pass it through degradation process, mixes AWG noise and produces blurred and noisy observations $g(x,y)$, which are sent to the Alternating Minimization model in order the restore the original information out of these noisy and blurred observations.
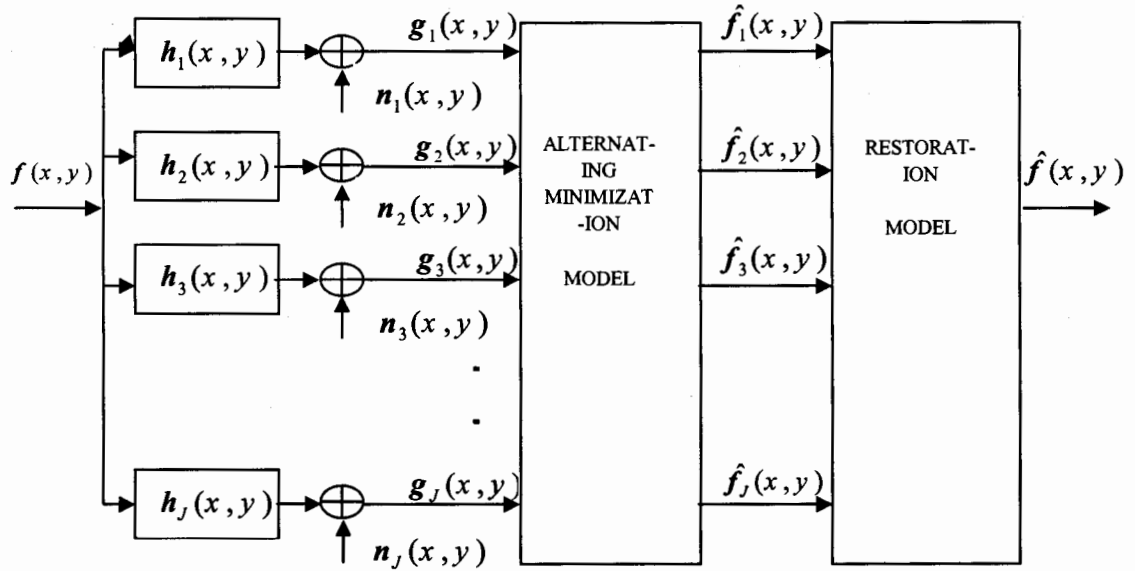
Figure 4.2: Internal structure of Observation Model

As discussed earlier, the above mentioned problem can also be represented in Matrix-Vector form, which can be seen from equation (3.3). Now the vectors g, f and n doesn't contain a single vector, rather they carry multiple vectors. This equation can be written in expanded form as,

$$
\begin{pmatrix} g_1(x,y) \\ g_2(x,y) \\ g_3(x,y) \\ . \\ . \\ . \\ g_J(x,y) \end{pmatrix} = \begin{bmatrix} \mathbf{H}_{(1)}(x,y) \\ \mathbf{H}_{(2)}(x,y) \\ \mathbf{H}_{(3)}(x,y) \\ . \\ . \\ . \\ \mathbf{H}_{(J)}(x,y) \end{bmatrix} (f) + \begin{pmatrix} n_1(x,y) \\ n_2(x,y) \\ n_3(x,y) \\ . \\ . \\ . \\ n_J(x,y) \end{pmatrix}
\tag{4.4}
$$

With $\mathbf{H} = [\mathbf{H}_1^T, \mathbf{H}_2^T, \ldots \ldots \mathbf{H}_J^T]$, $\mathbf{H}_l$ is the PSF matrix associated to h_l [35]. In order to view the structure of $\mathbf{H}$, let's take any arbitrary $\mathbf{H}_l$ matrix, its internal structure is shown below.

$$\mathbf{H}_l = \begin{bmatrix} [\mathbf{H}_1] & \cdots & 0 \\ \vdots & \ddots & \vdots \\ [\mathbf{H}_J] & \ddots & [\mathbf{H}_1] \\ \vdots & \ddots & \vdots \\ 0 & \cdots & [\mathbf{H}_J] \end{bmatrix} \qquad (4.5)$$

In order to observe the internal structure of each Toeplitz block, let $[\mathbf{H}_q]$ be a Toeplitz block taken from Block Toeplitz matrix $\mathbf{H}$, then $[\mathbf{H}_q]$ can be defined as,

$$[\mathbf{H}_q] = \begin{bmatrix} h(q,1) & \cdots & 0 \\ \vdots & \ddots & \vdots \\ h(q,K) & \ddots & h(q,1) \\ \vdots & \ddots & \vdots \\ 0 & \cdots & h(q,K) \end{bmatrix} \qquad (4.6)$$

It can be observed that a Toeplitz block $[\mathbf{H}_q]$ is associated to h_q. In this way $h(x,y)$ constitute the whole BTTB matrix.

4.2.3 Alternating Minimization Model

After receiving the degraded observations of original image, original image information has to be retrieved out of these blurred and noisy observations. For the purpose of deconvolution different algorithms have been discussed in chapter 3, but before we use any of it, problem statement and the assumptions have to be constructed which are needed to be applied on deconvolution problem.

Initially, a restoration approach will be developed for a single channel, and then it will generalize it for 'J' Channels. For the problem of restoring the original image out of blurred and noisy observation the model defined in equation (4.2) is consider

When the PSF '$\mathbf{H}$' performs convolution, its structure is of a Toeplitz matrix, and if it is zero padded, '$\mathbf{H}$' structure will represent a circulant matrix, and hence diagonalizable by the Discrete Fourier Transform (DFT) matrix. Let 'n' a additive Gaussian noise vector with zero mean, then the maximum likelihood estimator of f is the minimizer of the cost function

$$J(f) = \|\mathbf{H}f - g\|^2 \tag{4.9}$$

$$\textit{Lesso Estimator: } norm \mathbf{A} \ \square \ \left(\|\mathbf{A}\|^p\right)^{1/p} \ 1 < p < \infty \tag{4.10}$$

An assumption is made that the matrix '$\mathbf{H}$' is partially known, i.e. $\mathbf{H}_i = \mathbf{H}_0 + \varepsilon\Delta_i$, where 'i' represents the number of channels, and $\sum_{x,y} h(x,y) = 1$ where $\|\Delta\|_{\mathbf{w}} \ \square \ \|\mathbf{W}\Delta\| \leq \varepsilon$ and $\mathbf{W}$ is a smoothing matrix [41]. By replacing the value of $\mathbf{H}$ in the equation (4.9), we get

$$J(f) = \|(\mathbf{H}_0 + \varepsilon\Delta)f - g\|^2 \tag{4.11}$$

Since Δ is the part of $\mathbf{H}$ that is unknown, so in order to minimize the cost function, dependence on unknown parameters is needed to be removed. By using minimax criterion, that is, we look for the f which minimizes the maximum role of Δ, our cost function becomes

$$J(f) = \max_{\Delta} \ \|(\mathbf{H}_0 + \varepsilon\Delta)f - g\|^2 \ suchthat \ \|\Delta\|_W \leq \varepsilon \tag{4.12}$$

4.2.3.1 The sparse constraint

We have already explained that why the image is of sparse nature, so we have to apply sparse constraint on the restoring algorithm. The sparsity is defined as:

$$\|f\|_0 \square \sum_{i=1}^{n} I(f_i \neq 0) \tag{4.13}$$

Suppose that we are given a matrix $\tilde{\mathbf{H}}$ and we need to minimize the following objective function

$$\min_{f} \|\tilde{\mathbf{H}}f - g\|^2 \ suchthat \ \|f\|_0 \leq c \tag{4.14}$$

Where 'c' is any non-zero scalar number, this problem is combinatorial in nature, with a total of $\sum_{i=0}^{c} \binom{n}{i}$ possible solutions, and can be shown to be NP-hard. This type of problem can be solved employing convex relaxation to the problem. That is, if the l_0 constraint is replaced with l_1 constraint, and under certain conditions on $\tilde{\mathbf{H}}$, each formulation will result in same output. Therefore, we seek to minimize

$$\min_{f} \|\tilde{\mathbf{H}}f - g\|^2 \ suchthat \ \|f\|_1 \leq \tilde{c} \tag{4.15}$$

Now the method of constrained least squares is required to express this constrained problem as,

$$\hat{f} = \arg\min_{f} \|\tilde{\mathbf{H}}f - g\|^2 + \lambda \|f\|_1 \tag{4.16}$$

In order to get the argument minimum, we need to apply partial derivative as:

$$\frac{\partial \hat{f}}{\partial f} = \frac{\partial}{\partial f} \|\tilde{\mathbf{H}}f - g\|^2 + \frac{\partial}{\partial f} \lambda \|f\|_1 = 0 \tag{4.17}$$

$$\frac{\partial}{\partial f} 2(\tilde{\mathbf{H}}f - g)^{\mathrm{T}}(\tilde{\mathbf{H}}f - g) + \lambda \frac{\partial}{\partial f} 2f^{\mathrm{T}}f = 0$$

$$\frac{\partial}{\partial f}\left(f^{\mathrm{T}}\tilde{\mathbf{H}}^{\mathrm{T}}-y^{\mathrm{T}}\right)\left(\tilde{\mathbf{H}}f-g\right)+\lambda\frac{\partial}{\partial f}f^{\mathrm{T}}f=0$$

$$\tilde{\mathbf{H}}^{\mathrm{T}}\left(\tilde{\mathbf{H}}f-g\right)+\lambda f=0$$

$$\tilde{\mathbf{H}}^{\mathrm{T}}\tilde{\mathbf{H}}f-\tilde{\mathbf{H}}^{\mathrm{T}}g+\lambda f=0$$

$$\tilde{\mathbf{H}}^{\mathrm{T}}\tilde{\mathbf{H}}f+\lambda f=\tilde{\mathbf{H}}^{\mathrm{T}}g$$

$$\left(\tilde{\mathbf{H}}^{\mathrm{T}}\tilde{\mathbf{H}}+\lambda\mathbf{I}\right)f=\tilde{\mathbf{H}}^{\mathrm{T}}g$$

$$\hat{f}=\frac{\tilde{\mathbf{H}}^{\mathrm{T}}g}{\left(\tilde{\mathbf{H}}^{\mathrm{T}}\tilde{\mathbf{H}}+\lambda\mathbf{I}\right)}$$

$$\hat{f}=\left(\tilde{\mathbf{H}}^{\mathrm{T}}\tilde{\mathbf{H}}+\lambda\mathbf{I}\right)^{-1}\tilde{\mathbf{H}}^{\mathrm{T}}g \tag{4.18}$$

The solution of equation (4.18) can be also reached by using another approach as well, which is known as an iterative thresholding technique described in [36]. If we let 's' be the largest singular value of $\tilde{\mathbf{H}}$, the minimization can be achieved by minimizing with respect to each f_i, independently as

$$\hat{f}_i(n+1)=D_{\frac{\xi}{2}}([\hat{f}(n)+\tilde{\mathbf{H}}^{\mathrm{T}}\left(\frac{g}{s^2}-\tilde{\mathbf{H}}\hat{f}(n)\right)]_i) \tag{4.19}$$

Here $D_\theta(x)=(x-\operatorname{sgn}(x)\frac{\theta}{2})I(|x|\geq\frac{\theta}{2})$ is the soft thresholding operator and is used for the purpose of denoising.

4.2.3.2 The Smoothness Constraint

It has already been discussed that a smoothness penalty will be applied on allowable PSFs. Thus we seek to maximize the following cost function, while utilizing the constraints set out earlier, toward a minimax criterion. Hence objective function becomes

$$\hat{\delta} = \arg\max_{\delta} \left\| e + \varepsilon \mathbf{F}\delta \right\|^2 \ suchthat \ \left\| \mathbf{W}\delta \right\|^2 \leq \varepsilon \tag{4.20}$$

Here 'e' denotes the observation error vector i.e. $e = \mathbf{H}_0 f - g$. By transforming the problem into constrained least squares we can re-write the objective function as

$$\hat{\delta} = \arg\min_{\delta} - \left\| e + \varepsilon \mathbf{F}\delta \right\|^2 + \gamma \left\| \mathbf{W}\delta \right\|^2 \tag{4.21}$$

$$\frac{\partial \hat{\delta}}{\partial \delta} = \frac{\partial \left\| e + \varepsilon \mathbf{F}\delta \right\|^2}{\partial \delta} + \frac{\gamma \left\| \mathbf{W}\delta \right\|^2}{\partial \delta} = 0$$

$$\frac{\partial 2 \left(e + \varepsilon \mathbf{F}\delta \right)^T \left(e + \varepsilon \mathbf{F}\delta \right)}{\partial \delta} + \frac{\partial 2\gamma \left(\mathbf{W}\delta \right)^T \left(\mathbf{W}\delta \right)}{\partial \delta} = 0$$

$$\varepsilon \mathbf{F}^T \left(e + \varepsilon \mathbf{F}\delta \right) + \gamma \mathbf{W}^T \left(\mathbf{W}\delta \right) = 0$$

$$\varepsilon \mathbf{F}^T e + \varepsilon\varepsilon \mathbf{F}^T \mathbf{F}\delta + \gamma \mathbf{W}^T \mathbf{W}\delta = 0$$

$$\hat{\delta} = \frac{\varepsilon \mathbf{F}^T e}{\varepsilon^2 \mathbf{F}\mathbf{F}^T + \gamma \mathbf{W}^T \mathbf{W}}$$

$$\hat{\delta} = \varepsilon \left(\gamma \mathbf{W}^T \mathbf{W} - \varepsilon^2 \mathbf{F}\mathbf{F}^T \right)^{-1} \mathbf{F}^T e \tag{4.22}$$

4.2.3.3 Alternating Minimization Algorithm

The basic alternating minimization algorithm has been very successful in the context of solving optimization problems over two variables. The iterative nature and simplicity of the algorithm has led to its application to many areas. AM algorithm is used for quantitative image reconstruction for differential interference contrast (DIC) microscopy, in which it computes a specimen's complex transmittance function, both magnitude and phase, from DIC images . Blind equalization has been performed by using AM algorithm for the applications to mobile communications. AM algorithm is used for X-ray computed tomography and it is used for dual energy X-ray CT. After all the discussion we are now able to define the cost function as,

$$J(f,\delta) = \left\| (\mathbf{H}_0 + \varepsilon\Delta)f - g \right\|^2 = \left\| \mathbf{F}(h_0 + \varepsilon\delta) - g \right\|^2 \ such \ that \ \left\| f \right\|_1 \leq \tilde{c} \ and \ \left\| \mathbf{W}\delta \right\|^2 \leq \varepsilon$$

This cost function can also be expressed in AM suitable form as;

$$J(f,h) = \left\| \mathbf{H}f - g \right\|_2^2 + \lambda \left\| f \right\|_1 + \gamma \left\| \mathbf{W}\delta \right\|^2 \tag{4.23}$$

The alternating minimization algorithm minimizes the cost function $J(f,h)$ by iteratively solving the following sequence of optimization problems. If we are given $f_{est}(x,y)$, we will solve

$$h_i(x,y) = \arg\ \min_h\ J(f_{est},h),$$

Similarly if we are given $h_{est}(x,y)$ then we will solve

$$f_i(x,y) = \arg\min_f J(f,h_{est})$$

Where $f_{est}(x,y)$ and $h_{est}(x,y)$ denote the initial estimate of the original image and the point spread function respectively, and $h_i(x,y)$, $f_i(x,y)$ are the updated values based on the information provided by $f_{est}(x,y)$ and $h_{est}(x,y)$. Generally we set the initial estimate of the original image to the observed image, which is noisy and blurred i.e. $f_{est}(x,y)=g(x,y)$ where as PSF has been initialized with the smooth approximation of the original unknown PSF.

The AM algorithm follows the following algorithm in order to solve the image and PSF reconstruction problem.

1. We have to initialize $f(0)$ to any suitable estimate, $g(0)$ is initialized with observation 'g', and PSF $\mathbf{H}(0)$ is initialized with '$\mathbf{H}_0$' which is a smooth approximation of original PSF.

2. We need to update $f(n)$, for this purpose we will have to solve the equation

$$f(n+1) = \arg\min_f \|\mathbf{H}(n)f - g(n)\|^2 \; suchthat \; \|f\|_0 \leq p$$

The solution of this problem has already been explained in the equation (4.2.20)

3. In order to update 'f' we also need to update '$\mathbf{H}$' and 'g', which are given as

$$\mathbf{H}(n+1) = \left[\mathbf{I} + \varepsilon^2 f(n)\left(\gamma \mathbf{w}^\mathrm{T}\mathbf{w} - \varepsilon^2 f^\mathrm{T}(n)f(n)\right)^{-1} f^\mathrm{T}(n)\right]\mathbf{H}_0$$

$$g(n+1) = \left[\mathbf{I} + \varepsilon^2 f(n)\left(\gamma \mathbf{w}^\mathrm{T}\mathbf{w} - \varepsilon^2 f^\mathrm{T}(n)f(n)\right)^{-1} f^\mathrm{T}(n)\right]g$$

4. When the stopping criterion is met, we get the output estimated '$\hat{f}(x,y)$'.

5. In order to restore $\mathbf{H}$, this estimated '$\hat{f}(x,y)$' is transformed into 'F', as explained earlier. Now we have the cost function as, $\hat{\delta} = \arg\min \left\| \hat{\mathbf{F}} h - g \right\|^2 + \tilde{\gamma} \left\| \mathbf{W}\delta \right\|^2$, the solution to this is given by equation (4.22). Matrix 'Δ' can be formed from $\hat{\delta}$ by following the equation (4.9). We will calculate $\mathbf{H}_i = \mathbf{H}_0 + \varepsilon\Delta_i$

In AM algorithm, the optimal estimates of $f(x,y)$ and $h(x,y)$ are obtained when we terminate the iterations after certain stopping criteria is fulfilled, it can be the number of iterations performed or if the error difference gets minimized i.e. the error norms $\left\| f_i - f_{i-1} \right\|_2$ and $\left\| h_i - h_{i-1} \right\|_2$ becomes smaller than the predefined constant.

In order to ensure the convergence of AM algorithm to suitable approximates, we can set some useful constraints on the algorithm iterations, based on the information which is already known, for example, we can set a constraint on the approximated PSF and original image that they cannot contain any negative values.

Also to ensure the convergence we apply the constraint that the sum of the values of the PSF will result in unity i.e.

$$\sum_{x,y} h(x,y) = 1 \tag{4.24}$$

Furthermore the constraints such as sparsity constraint and smoothness constraint have been explained earlier.

The parameter of success for any algorithm is how efficient is it in both executable time and convergence issues. Therefore, analysis of the convergence behavior for the

AM algorithm is crucial for understanding which local minimizer leads to AM convergence and how this minimizer depends on the initial guesses for original image $f(x,y)$ and PSF $h(x,y)$. It has been proven in [37], that AM algorithm converges to a local minimizer for any given initial guess and that it produces a very good restored image after only a few AM iterations.

After all the processing performed in ALTERNATING MINIMIZATION MODEL, we will get the estimated '$\hat{f}$' and '$\hat{H}$' against each channel as its output. These outputs are then sent to RESTORATION MODEL for further processing.

4.2.4 Restoration Model

The multiple restored images extracted from 'J' different degraded observations are then placed in the Restoration Model. The purpose of Restoration Model is to provide us a single image out of multiple restored images such that this image will be considered as the final estimated $\hat{f}$, which has been restored out of multiple degraded observations.

The Alternating Minimization is robust to noise and from simulations and results we have seen that the AM algorithm has successfully restored the images out of degraded observations. This leads us to propose a way to select the final estimated $\hat{f}$ out of multiple restored outputs provided by Alternating Minimization Model.

Since we do not have any prior information about the original image, hence we cannot utilize the traditional ways to measure the error of the restored image. In order to

select a single estimated $\hat{f}$ out of multiple estimated $\hat{f}$'s we will take average of all other estimations.

$$\hat{f} = \frac{\sum\limits_{i=1}^{J} \hat{f}_i}{J} \tag{4.25}$$

Where $i=1,2.....J$ is the number of channels, $\hat{f}_i$'s are the multiple restored images provided by the Alternating Minimization block and J represents the total number of channels. Hence in this way we will be able to select a single $\hat{f}$ out of multiple restored images.

CHAPTER 5

SIMULATIONS AND RESULTS

In this chapter the results originated by simulating the Alternating Minimization algorithm for the purpose of restoring the original image out of degraded observations will be discussed. The convergence issues of A.M algorithm and the effect of denoising parameter in the convergence of the algorithm shall also be observed. A.M algorithm shall be analyzed under controlled environment on the basis of evaluation parameters, such as Mean Square error, Normalized MSE, Signal to Noise ration and Improved S.N.R. The performance of proposed multichannel blind image deconvolution shall also be observed.

5.1   Convergence of A.M algorithm

Here it has been shown the way A.M algorithm restores the original image out of the degraded observation. Since A.M algorithm is an iterative algorithm which updates its parameters after each iteration by keeping in view the applied constraints. In order to show step by step performance of A.M algorithm an input image has been distorted

with additive white Gaussian noise of zero mean and SNR 40dB. The blurring effect is caused by system's PSF and the image gets distorted because of the additive noise. Now in figure 5.1 the progress of A.M algorithm is shown after specific number of iterations and at a fixed denoising parameter.
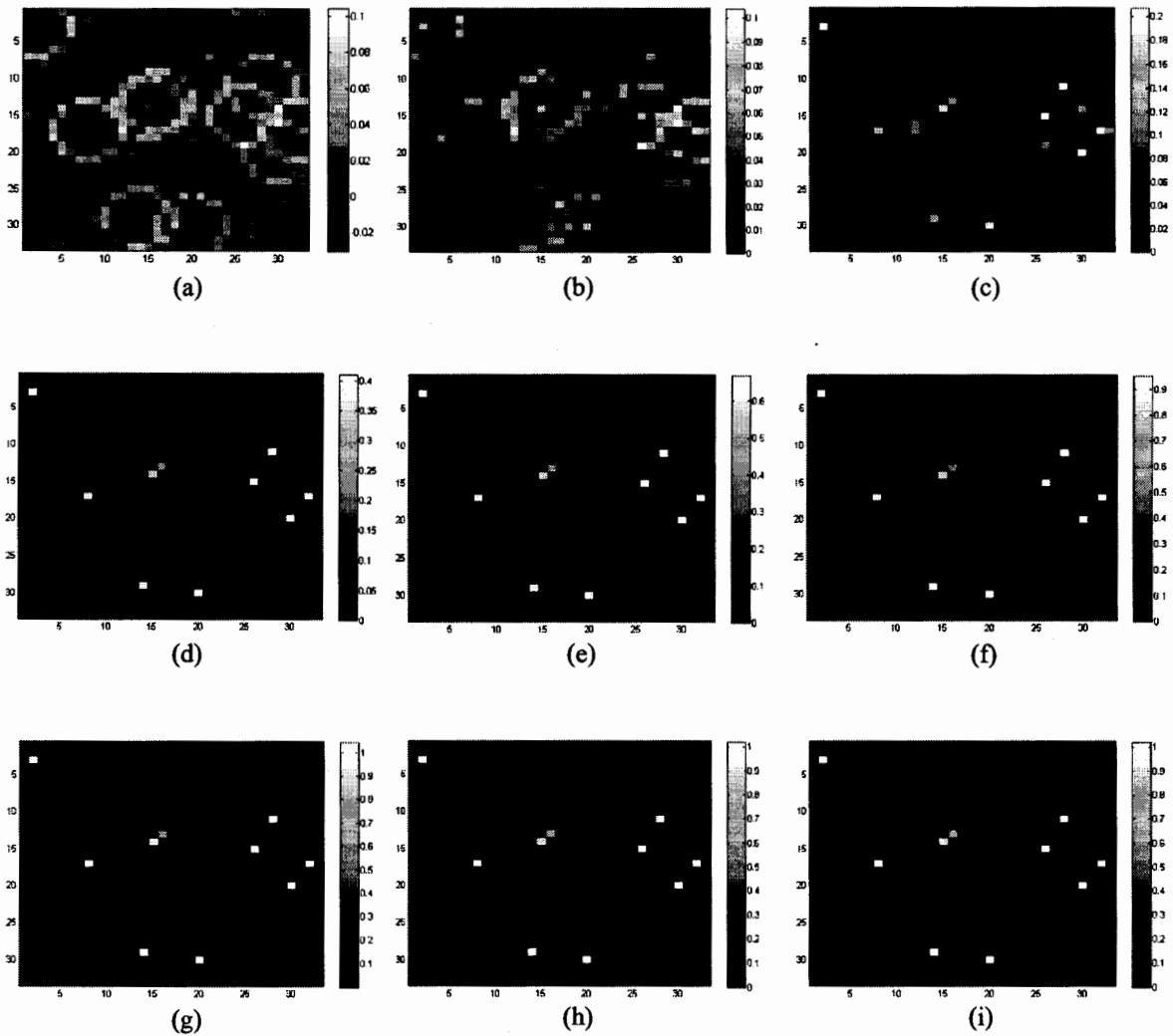

Figure 5.1 Degraded image and Blind image deconvolution images with denoising parameter 'ξ' 0.0120 at different iterations using AM algorithm (a) Degraded observation with noise SNR 40dB (b) Restored image at 5 iterations (c) Restored image at 20 iterations (d) Restored image at 50 iterations (e) Restored image at 100 iterations (f) Restored image at 200 iterations (g) Restored image at 300 iterations (h) Restored image at 500 iterations (i) Restored image at 1000 iterations

An error graph has also been plotted in order to observe the convergence rate of the algorithm. The graph is plotted between error occurrence which can be determined as a difference between original image and restored image, and the number of iterations.
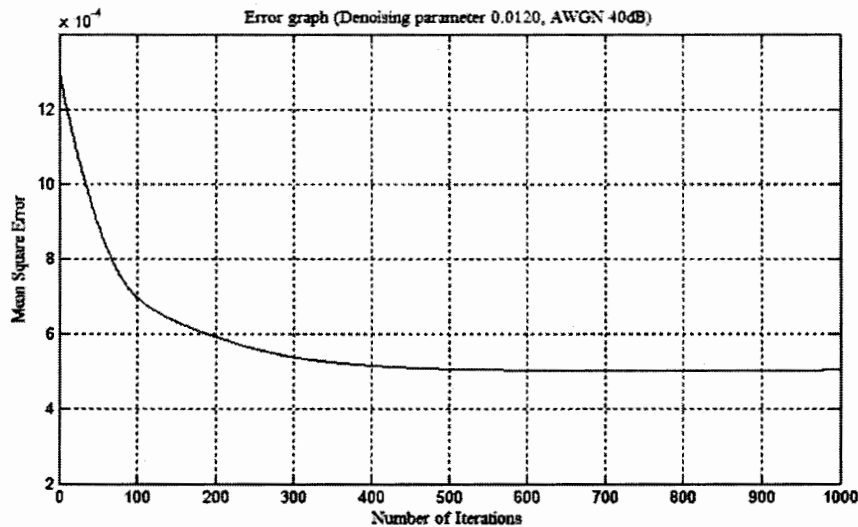

Figure 5.2 Error graph showing difference between original image f and restored image $\hat{f}$

In this simulation the SNR of noise has been set as 40dB, the denoising parameter 'ξ' is set to 0.0120 and the program is run for 1000 iterations. In figure 5.1 the behavior of A. M. algorithm is being shown in form of results at different iterations. The figure 5.1(a) shows the degraded observation, for the test purpose we know that this image is blurred because of convolution noise and is distorted with additive Gaussian noise of SNR 40dB. By observing these images it can be said that after 50 iterations, the algorithm reconstructed the points of interest but there is still some unwanted noise at the background. In figure 5.1(g) which shows result after 300 iterations, it can easily be concluded that the image has been successfully restored with only a few pixels

containing unwanted values. Similarly from figure 5.2, which shows us the error graph of the restored image with the original image, it can be seen that after 400 iterations the error graph has reached at a stable state. The figure 5.1 (i), shows result after 1000 iterations, other than points of interest some pixels still contains nonzero values, these values can be ignored since they are of very small intensities when compared to the points of interest.

5.2   Robustness of A.M Algorithm

Now the robustness of A.M algorithm shall be observed against additive white Gaussian noise. This is performed by generating the degraded observations with the help of noise having different intensities, by virtue of which it will distort the original image in different ways depending upon its intensity. This will show us the behavior of AM algorithm against different noise levels. The role of the denoising parameter ' ξ' will also be observed by altering its values in the algorithm. Error graphs will be plotted for different values of noise and denoising parameter ' ξ' with the help of which any change in the convergence behavior of the algorithm can easily be noticed.

First of all the denoising parameter ' ξ' will be initialized as 0.0128, the number of iterations to be performed are kept 1000 and the original image is degraded by noise of SNR 30dB, 35 dB, 40dB, 45dB, 50dB and 60dB as shown in the figures 5.3 and 5.4. The restored images are also shown in these figures below their corresponding degraded input.
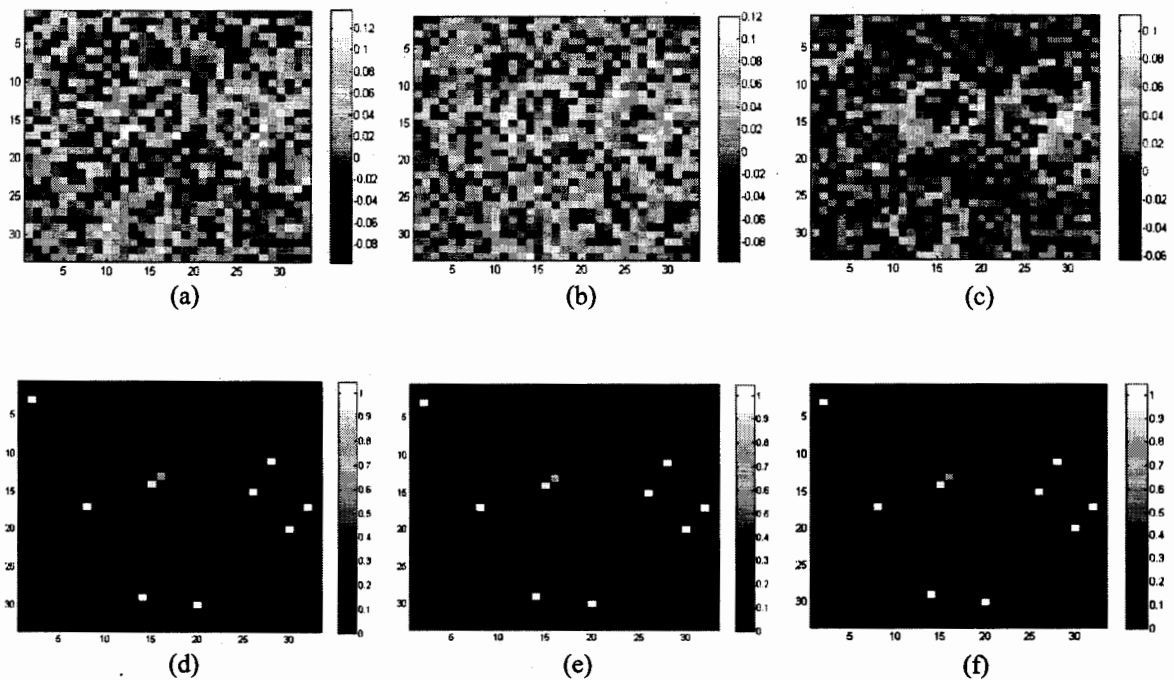
Figure 5.3 Degraded observations and restored images with noise SNR 30dB,35dB and 40dB
(a) Degraded observation with noise of SNR 30dB (b) Degraded observation with noise of
SNR 35dB (c) Degraded observation with noise of SNR 40 dB (d, e, f) Restored images out
of observations (a), (b) and (c) respectively.

In the figure 5.3, additive white Gaussian noise is shown with three intensity levels;
figure 5.3(a) represents the observation with noise of SNR 30dB. It can be seen that at
this noise level we can hardly find any information about the original image, yet AM
algorithm has successfully restored the original image, which can be seen in figure 5.3
(d). The figure 5.3 (b) and (e) shows degraded image with noise at 35dB and the
restored image respectively. Similarly figure 5.3 (c) and (f) represents the degraded
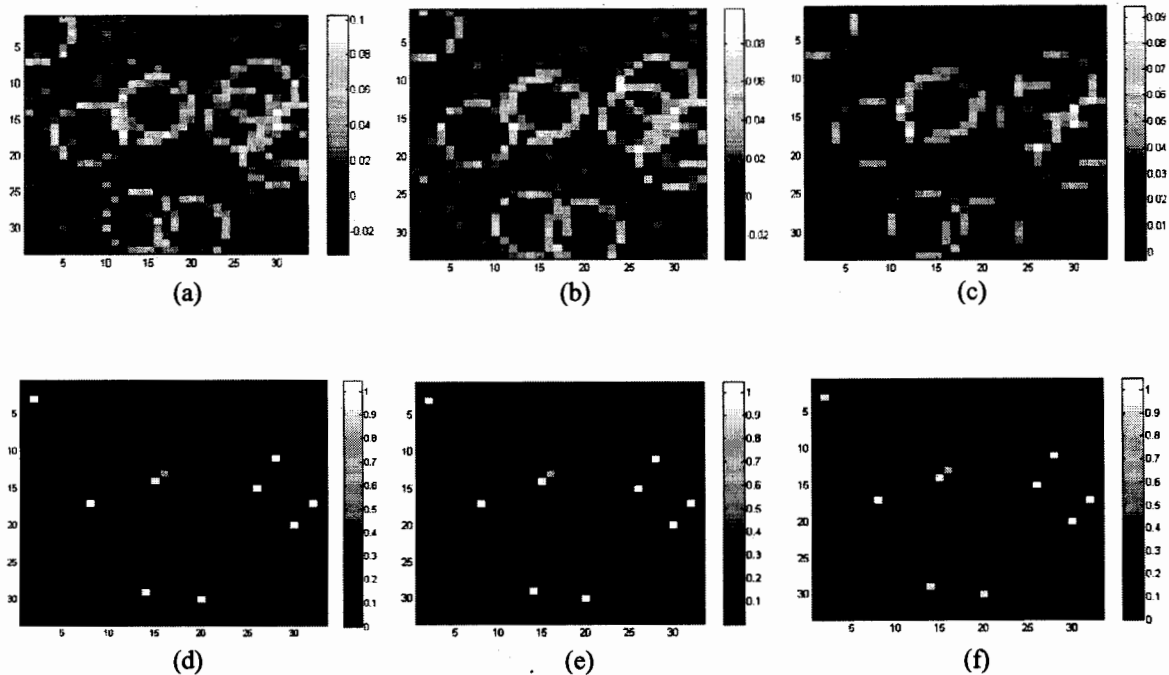image with noise at 40 dB and the restored image respectively.

Figure 5.4 Degraded observations and restored images with noise SNR 45dB, 50dB and 60dB (a) Degraded observation with noise of SNR 45 dB (b) Degraded observation with noise of SNR 50dB (c) Degraded observation with noise of SNR 60dB (d, e, f) Restored images out of observations (a), (b) and (c) respectively.

The figure 5.4 (a) represents the degraded image with noise of SNR 45dB and figure 5.4(d) represents the restored image by the algorithm. Degraded image with SNR 50dB noise is shown in figure 5.4(b) and its corresponding restored image is shown in figure5.4 (e). Similarly figure 5.4(c) and (f) represents the degraded image with noise of SNR 60dB and restored image respectively.

From this experiment it can be concluded that A.M algorithm is robust for the above mentioned noise intensities and has successfully restored all the images out of degraded observations. Since the A.M algorithm has been tested on a wide range of noise intensities, varying from 30dB to 60dB and the A.M algorithm has restored the images successfully, now the role of denoising parameter ' ξ ' shall be observed in the

convergence of this algorithm and only three noise intensities will be used in these experiments i.e. 30dB, 40dB and 50dB.

Now the denoising parameter 'ξ' is initialized as 0.016, the iterations to be performed are kept as 1000 and the noise intensities to be used for the degradation of original image are set as 30dB, 40dB and 50dB. The degraded inputs and their corresponding restored images are shown in figure 5.5

Figure 5.5: Degraded observations and restored images using ξ=0.016 (a) Degraded observation with noise of SNR 30dB (b) Degraded observation with noise of SNR 40dB (c) Degraded observation with noise of SNR 50dB (d),(e) and (f) Restored images out of observations (a), (b) and (c) respectively.

Now the denoising parameter 'ξ' is initialized as 0.0352, the iterations to be performed are kept as 1000 and the noise intensities to be used for the degradation of original image are set as 30dB, 40dB and 50dB. The degraded inputs and their corresponding restored images are shown in figure 5.6
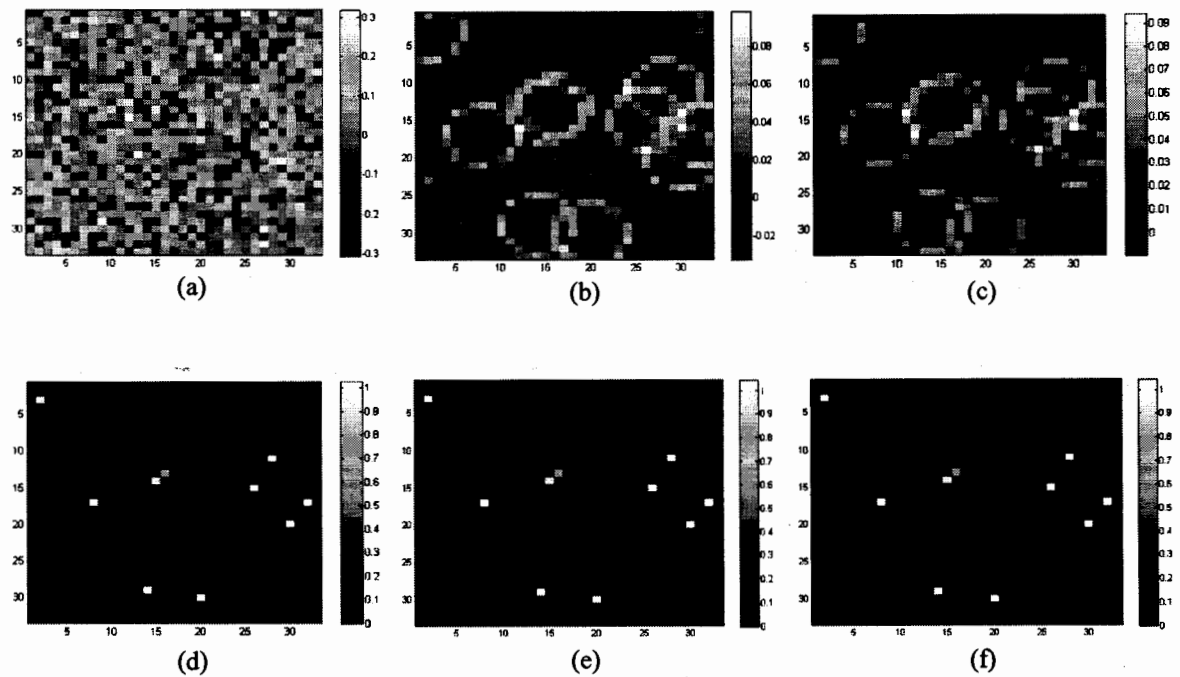
Figure 5.6: Degraded observations and restored images using ξ=0.0352 (a) Degraded observation with noise of SNR 30dB (b) Degraded observation with noise of SNR 40dB (c) Degraded observation with noise of SNR 50dB, (d, e, f) Restored images out of observations (a), (b) and (c) respectively.

Now the denoising parameter 'ξ' is set as 0.06, the iterations to be performed are kept as 1000 and the noise intensities to be used for the degradation of original image are set as 30dB, 40dB and 50dB. The degraded inputs and their corresponding restored images are shown in figure 5.7
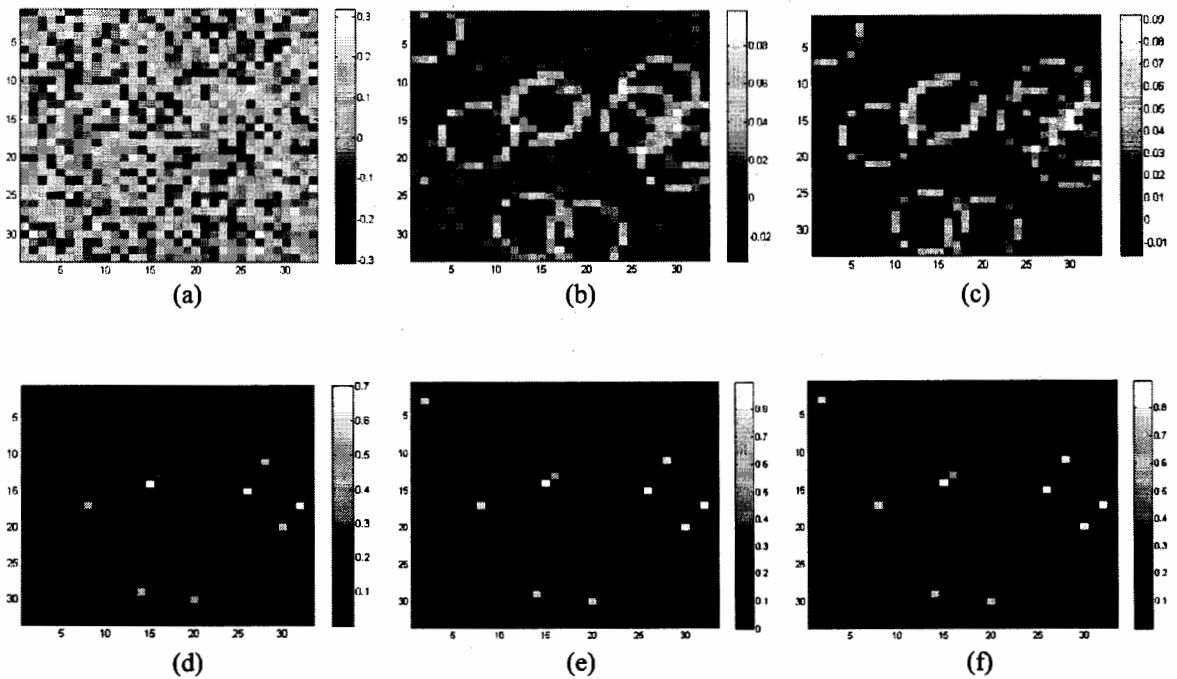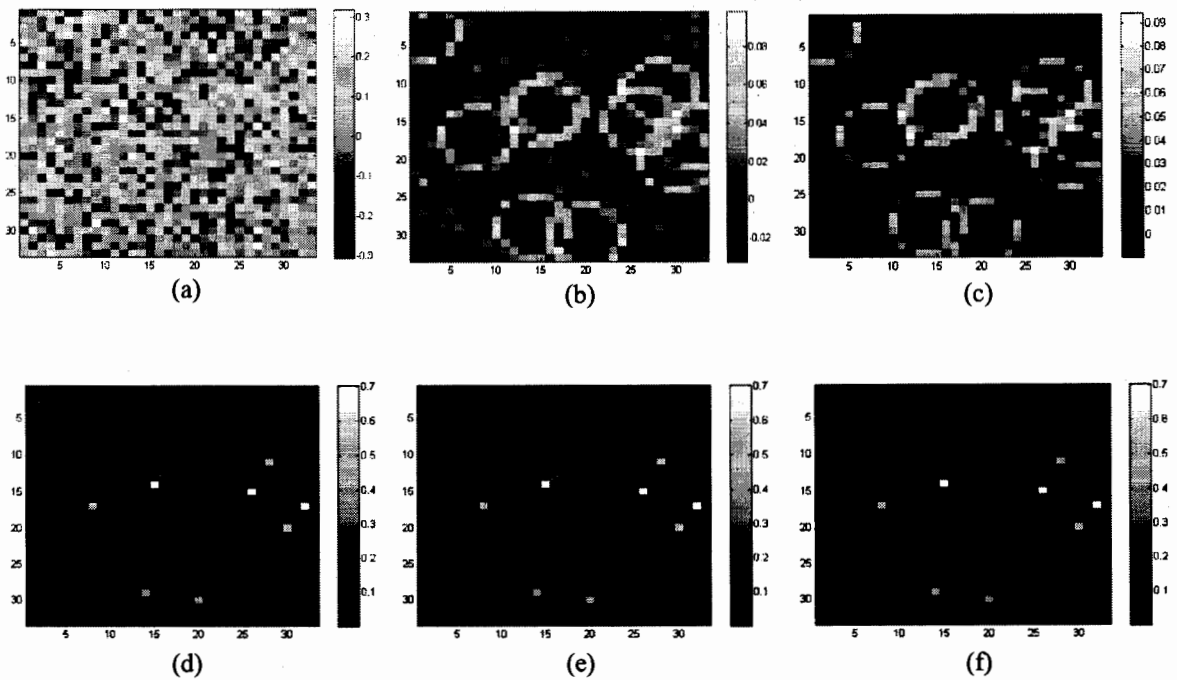
Figure 5.7: Degraded observations and restored images using ξ=0.06 (a) Degraded observation with noise of SNR 30dB (b) Degraded observation with noise of SNR 40dB (c) Degraded observation with noise of SNR 50dB (d, e, f) Restored images out of observations (a), (b) and (c) respectively.

In order to observe the effect of choosing the denoising parameter, the mean square error graphs of different denoising parameters have been plotted by keeping number of iterations and noise intensity constant. With the help of these graphs any change in the quality of the recovered images can be analyzed.

These graphs have been plotted for three different Signal to Noise Ratios, i.e. 30dB, 40dB and 50dB, number of iterations to be performed are kept as 1000 and five different denoising parameters have been used in order to analyze the performance of the algorithm.
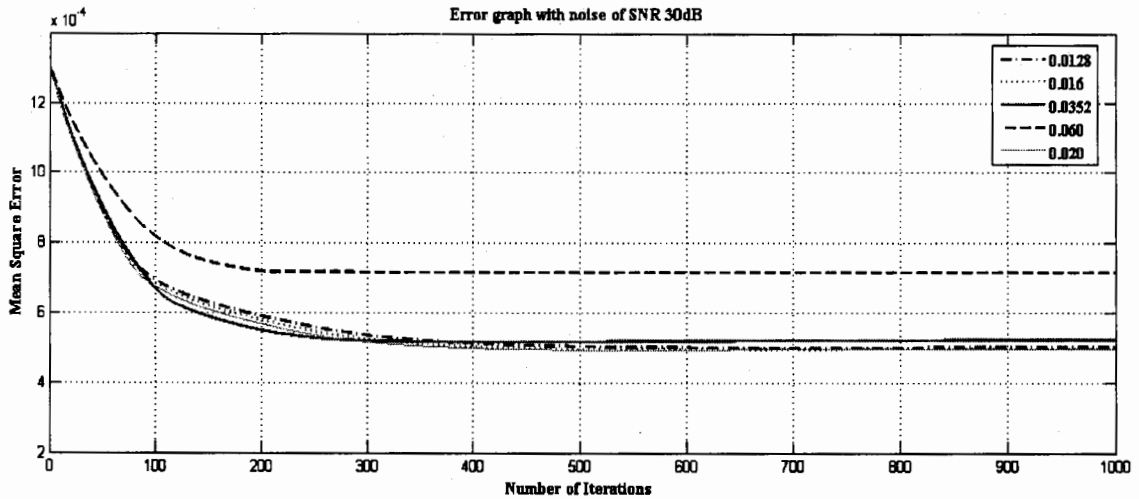
Figure 5.8: Error plot shows rate of convergence of A.M algorithm using degraded observation having noise of SNR 30dB with noise parameters ξ=0.016, ξ=0.0128, ξ =0.0352, ξ=0.020 and ξ=0.06.

In figure 5.8, noise SNR is set to 30dB, number of iterations performed are 1000 and five different denoising parameters are used. We can observe from the graph that denoising parameter ξ=0.06 has quickly got into a stable state as compared to others however it has produced larger error. Same is the case with ξ=0.0352, it has attained a steady state soon after 200 iterations but error has decreased in a significant manner. Whereas ξ=0.016, ξ=0.0128 and ξ=0.020, have taken more time to achieve a steady state but they have produced minimum error when compared with other graphs.

Figure 5.9: Error plot shows rate of convergence of A.M algorithm using degraded observation having noise of SNR 40dB with noise parameters ξ=0.016, ξ=0.0128, ξ =0.0352, ξ=0.020 and ξ=0.06.

In figure 5.9, noise SNR has been initialized with 40dB, number of iterations performed are 1000 and five different denoising parameters are used. This graph shows us that ξ=0.020 has produced minimum error but it has taken more time to attain a steady state than all other graphs. Other denoising parameters have also produced lesser error as compared to the error they have produced earlier with 30dB noise.
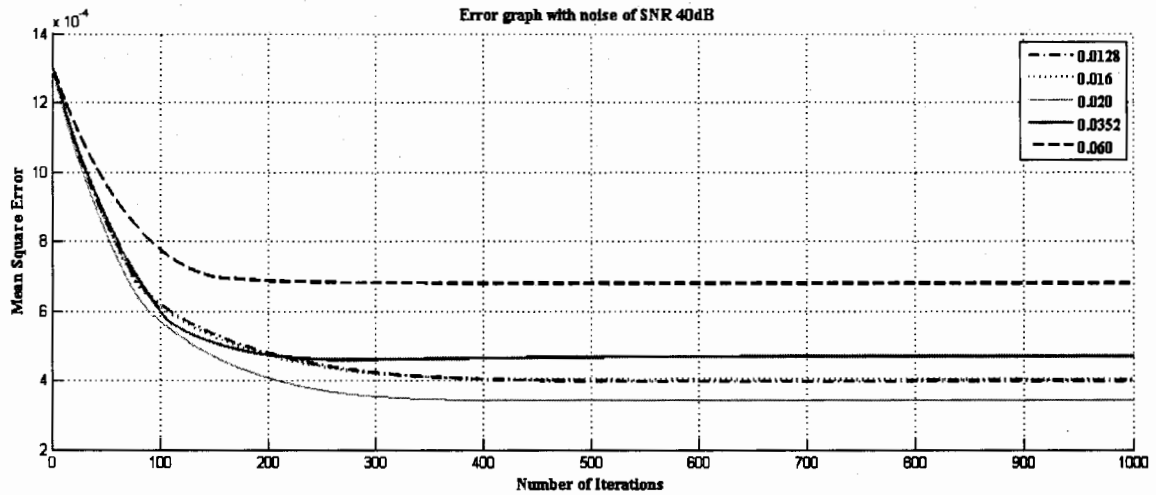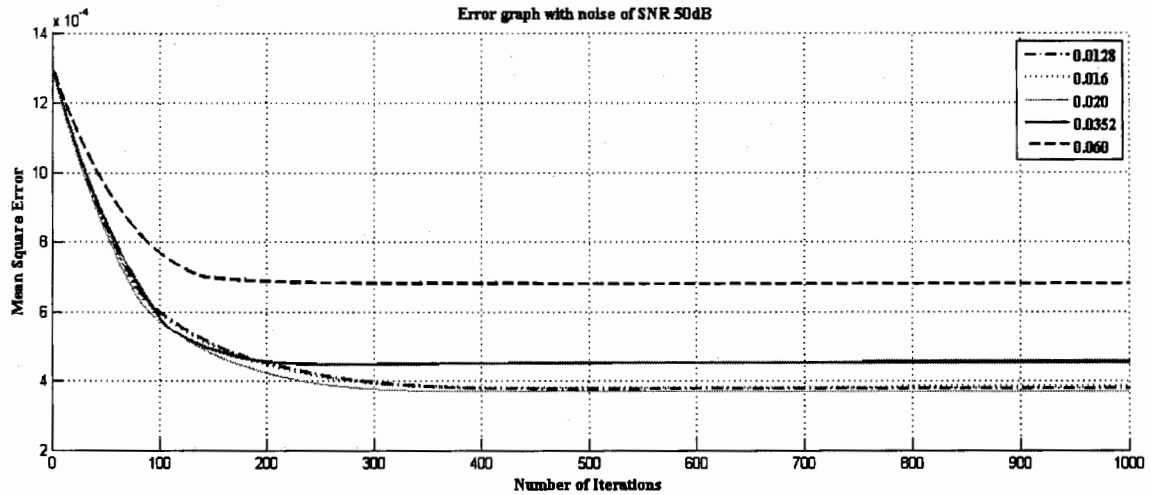
Figure 5.10: Error plot shows rate of convergence of A.M algorithm using degraded observation having noise of SNR 60dB with noise parameters ξ=0.016, ξ=0.0128, ξ =0.0352, ξ=0.020 and ξ=0.06.

In figure 5.10, ξ=0.0352 has shown quicker rate of convergence and also has produced lesser error than it has produced earlier for noise with SNR 30dB and 40dB while other denoising parameter have not been able to show significant loss in error. By observing the above mentioned results it can be concluded that denoising parameter ξ=0.020 has produced minimum errors in all three noise intensities.

5.3 Evaluation Parameters

In order to evaluate the performance and robustness of A.M algorithm the following parameters will be used. On the basis of this evaluation the best denoising parameter ' ξ' can be selected which will later be utilized for the multichannel blind image deconvolution scenario.

Mean Square Error

Table 5.1: Mean square values of degraded images

Denoising Parameter	SNR =30dB	SNR =40dB	SNR =50dB
0.0128	6.3862e-004	2.8413e-004	2.4065e-004
0.0160	6.3395e-004	2.8646e-004	2.4412e-004
0.020	6.3205e-004	2.3308e-004	2.3536e-004
0.0352	1.100e-003	8.2164e-004	7.8747e-004
0.0600	3.000e-003	2.800e-003	2.800e-003

Root Mean Square Error

Table 5.2: Root Mean square values of degraded images

Denoising Parameter	SNR =30dB	SNR= 40dB	SNR =50dB
0.0128	0.0253	0.0169	0.0155
0.0160	0.0257	0.0169	0.0159
0.020	0.0251	0.0152	0.0153
0.0352	0.0325	0.0287	0.0281
0.0600	0.0548	0.0532	0.0529

Above mentioned parameters give us information about the denoising parameters regarding the error they have produced. By observing these results it can be concluded that denoising parameter ξ=0.020 has produced minimum error than all other denoising parameters.

Signal to Noise Ratio

Table 5.3: Signal to noise ratio of degraded images

Denoising Parameter	SNR =30dB	SNR= 40dB	SNR= 50dB
0.0128	7.5979	11.1151	11.8365
0.0160	7.6298	11.0797	11.7743
0.020	7.4664	11.9381	11.6130
0.0352	5.4236	6.5035	6.6880
0.0600	0.8752	1.1241	1.1797

Improved SNR

Table 5.4: Improved SNR values of degraded images

Denoising Parameter	SNR 30dB	SNR 40dB	SNR 50dB
0.0128	4.7812	6.2132	6.4771
0.0160	4.7942	6.1988	6.4844
0.020	4.8092	6.3855	6.5000
0.0352	3.8918	4.3268	4.4038
0.0600	2.4827	2.5989	2.6285

The parameters such as Signal to Noise ratio and Improved SNR provide information regarding the quality of recovered image. These parameters have lead us to select denoising parameter '$\xi = 0.020$' as the best out of all other denoising parameters which were used in the simulation.

5.4   Proposed method results

Now for the proposed method's results, two examples have been discussed. In the first example the original image is produced by randomly selecting the nine non zero data points where as in second example the original image represents the sparse image of the Benzyl Benzene molecule.

Let's consider the case when imaging system has acquired three images of a sample. These three images have passed through three different channels and each channel has applied its own PSF and different intensity of noise distorts each channel as explained in figure 4.2.

As a result channel noise and AWGN noise, the observed images results in degraded images. Now these images need to be processed so that the original sent image and the point spread function could be retrieved out of these degraded observations. For this purpose A.M algorithm will be applied on these degraded observations and by using the proposed method final estimated image '$\hat{f}$' and point spread function '$\hat{H}$' will be restored.
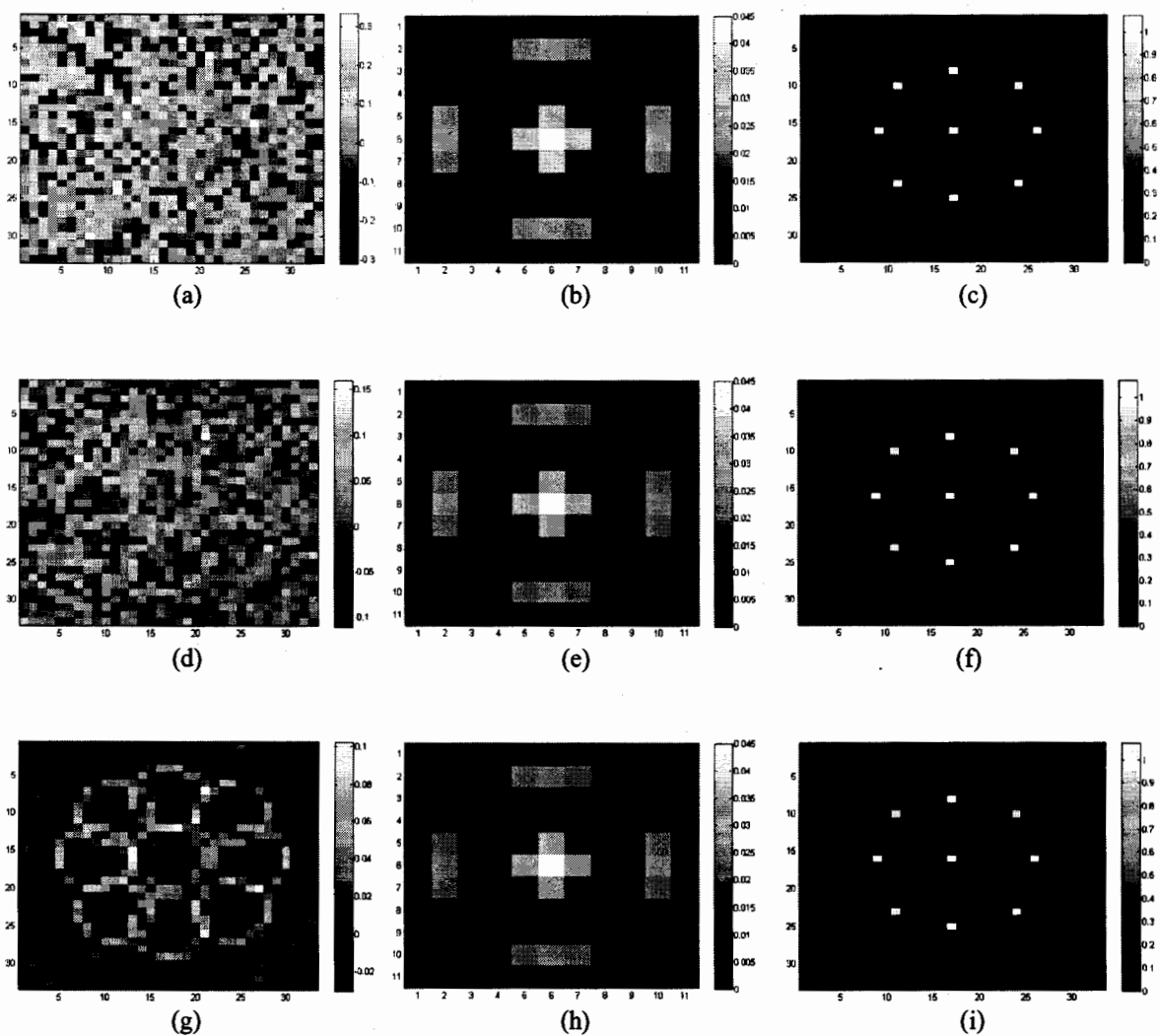
Figure 5.11 Multichannel degraded images and Blind image deconvolution images with denoising parameter 'ξ' 0.020 at 1000 iterations using AM algorithm (a) Degraded observation of channel 1 (b) Partially known PSF used in algorithm (c) Restored image of channel 1(d) Degraded observation of channel 2 (e) Partially known PSF used in algorithm (f) Restored image of channel 2 (g) Degraded observation of channel 3 (h) Partially known PSF used in algorithm (i) Restored image of channel 3.

In figure 5.11, images (a), (d) and (g) represents the output of channel 1, 2 and 3 respectively. Whereas the images (b), (e) and (h) represent the partially known part of system's PSF. Images (c), (f) and (i) represent the restored images by A.M algorithm. The output of RESTORATION MODEL shows only one estimated output, hence following the proposed method given by equation 4.25, average of these three images will be taken. The final restored image is shown in figure 5.11
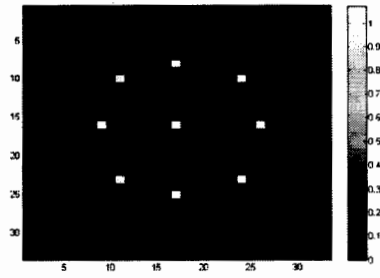
Figure 5.12: Restored output '$\hat{f}$' of Multichannel blind image deconvolution model

On the basis of this restored image, now PSF will have to be restored. In order to restore PSF equation 4.24 is solved, it will result in a vector $\hat{\delta}$, this $\hat{\delta}$ will be transformed into Block Circulant matrix Δ by using the equation 3.10. The matrix $\mathbf{H}$ is defined in equation 4.25, hence by setting ε to 1 and replacing the calculated value of Δ the estimated PSF $\hat{\mathbf{H}}$ will be calculated. The figure 5.13 shows the estimated $\hat{\mathbf{H}}$.
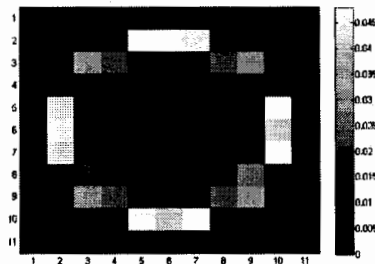

Figure 5.13: Restored output '$\hat{\mathbf{H}}$' of Multichannel blind image deconvolution model

In this second experiment, three images are acquired of the sample, these images are different from one another because of time varying point spread function and different intensity of atmospheric noise distorts the acquired image in different way.
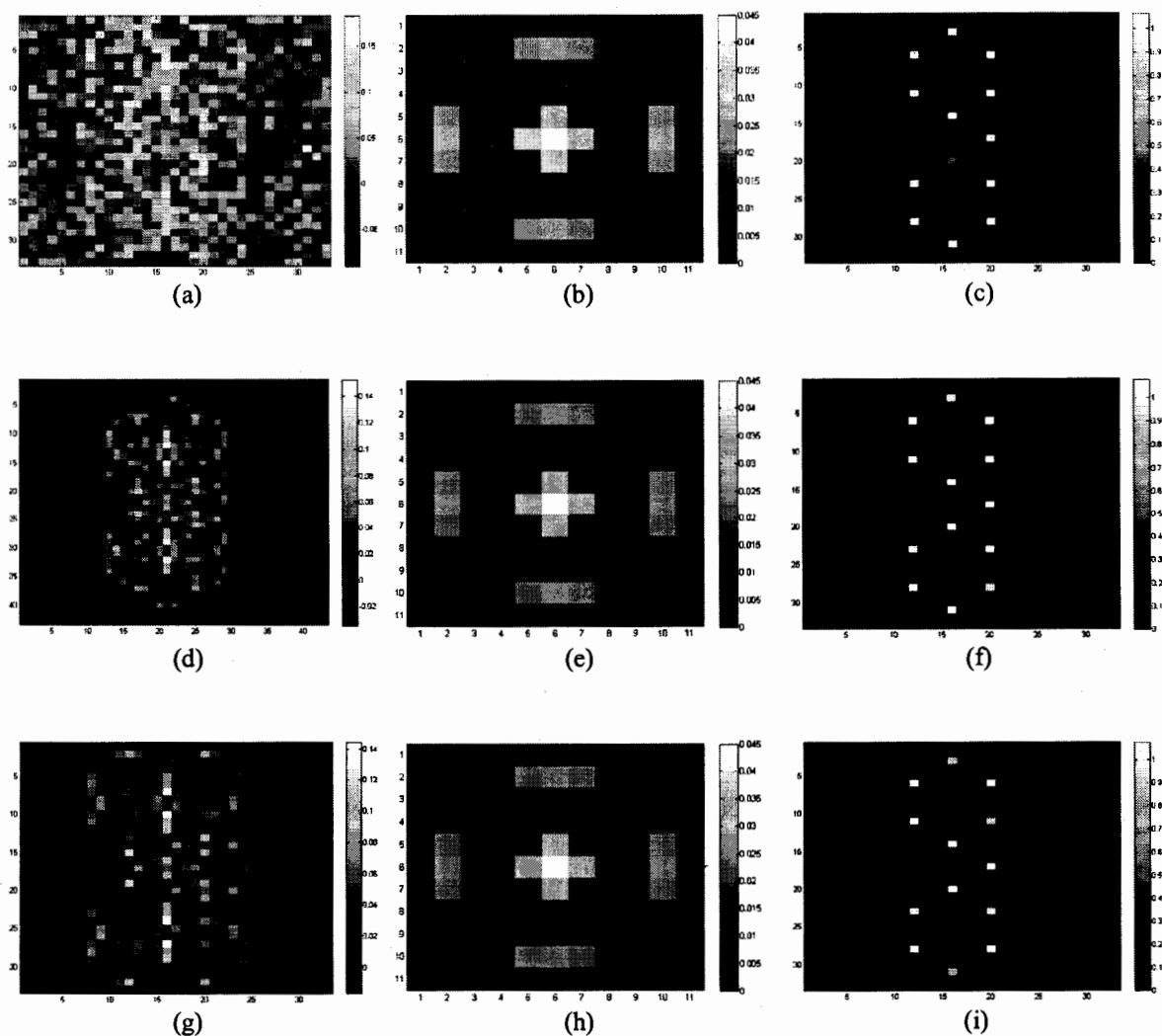
Figure 5.14 Multichannel degraded images and Blind image deconvolution images with denoising parameter 'ξ' 0.020 at 1000 iterations using AM algorithm (a) Degraded observation of channel 1 (b) Partially known PSF used in algorithm (c) Restored image of channel 1(d) Degraded observation of channel 2 (e) Partially known PSF used in algorithm (f) Restored image of channel 2 (g) Degraded observation of channel 3 (h) Partially known PSF used in algorithm (i) Restored image of channel 3.

In figure 5.14, images (a), (d) and (g) represents the degraded observations produced by channel1, channel2 and channel3 respectively. Images (b), (e) and (h) represents the approximated point spread function which is being used in order to retrieve original sent image and point spread function. Images (c), (f) and (i) represents the

output of the Alternating Minimization Model. The final estimated $\hat{f}$, which resulted after applying proposed method in RESTORATION BLOCK, is shown in figure 5.15.
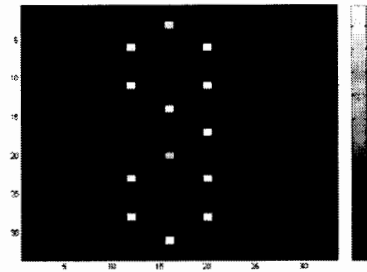

Figure 5.15: Restored output '$\hat{f}$' of Multichannel blind image deconvolution model

The final restored image $\hat{f}$ represents the sparse image in the shape of a Benzyl Benzene molecule. As explained in previous example, this estimated $\hat{f}$ will now be used in retrieving the point spread function of MRFM. The figure 5.16 shows the point spread function restored by using figure 5.15.
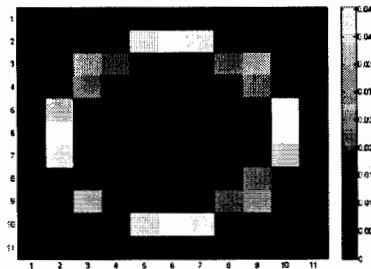

Figure 5.16: Restored output '$\hat{H}$' of Multichannel blind image deconvolution model

Observing the results, it can be stated that, A. M algorithm is proven robust against noise and it has achieved minimum mean square error very quickly hence settles itself into a steady state. In both examples, the proposed method has also successfully restored the original image and system's PSF.

CHAPTER 6

CONCLUSION AND FUTURE DIRECTIONS

The Alternating Minimization algorithm has been evaluated on the basis of certain parameters in order to observe its convergence rate and behavior in different intensities of degraded observations. A proposed method has been presented in order to solve Multichannel Blind Image Deconvolution problem.

6.1 Summary of results

Since iterative soft thresholding has been used for the purpose of denoising, the A.M algorithm was repeatedly tested by varying the denoising parameter 'ξ'. The results have shown that A.M algorithm has successfully restored the original images from all the degraded observations. Observing the results and evaluation parameters, it can be concluded easily that A.M algorithm has proved out to be robust against different noise intensities. The proposed approach for Multichannel Blind Image deconvolution has worked in significant manner and in both examples, the original sent image and system PSF, has been restored successfully.

6.2 Future Directions

These experiments has shown us the need of a method which could lead us to the optimal value of denoising parameter ' ξ '. Since we have seen how diverse the results could be if the denoising parameter ' ξ ' is not set appropriately.

In this thesis Alternating Minimization algorithm has been used for the purpose of Multichannel Blind Image Deconvolution, for further research algorithms such as Particle Swarm Optimization (PSO) or Genetic algorithms (GA) can also be utilized.

Furthermore for the Multichannel Blind Image Deconvolution problem, research can be done in order to exploit image diversity. Such techniques should be devised which can extract information from the multiple restored images and on the basis of that information the original image should be restored.

References

[1] J. L. Starck and E. Pantin, "Deconvolution in Astronomy: A Review," Publications of the Astronomical Society of the Pacific, No.114, pp. 1051-1069, 2002.

[2] M. Cannon, "Blind deconvolution of spatially invariant image blurs with phase," IEEE Transactions Acoustics, Speech and Signal Processing, Vol. 24(1), pp. 58-63, 1976.

[3] A. G khurshudov, K. Kato and H. Koide, "Wear of AFM diamond Tip sliding against silicon," Wear 203-204, 1997.

[4] N. H. Malsch, "Biomedical Nanotechnology," CRC Press, 2005.

[5] J. A. Sidles, J. L. Garbini, K. J. Bruland, D. Rugar, O. Zuger, S. Hoen and C. S. Yannoni, "Magnetic resonance force microscopy," Review of Modern Physics 67, No. 1, pp. 249-265, 1995.

[6] D. Rugar, R. Budakian, H. J. Mamin, and B. W. Chui, "Single spin detection by magnetic resonance force microscopy," Nature 430 , No. 6997, pp. 329-332, 2004.

[7] M. Ting, "Signal Processing for Magnetic Resonance Force Microscopy," PhD thesis, University of Michigan, 2006.

[8] K. Herrity, R. Raich, and A. O. Hero III, "Blind deconvolution for sparse molecular imaging," IEEE International Conference on Acoustics, Speech and Signal Processing, 2008.

[9]   R. Raich and A. O. Hero III, "Sparse image reconstruction for partially known blur functions," IEEE International Conference on Image Processing, pp. 637-640, 2006.

[10]   M. Ting, R. Raich, and A. O. Hero III, "Sparse image reconstruction using sparse priors," IEEE International Conference on Image Processing, pp. 1261-1264, 2006.

[11]   D. Kundur and D. Hatzinakos, "Blind Image Deconvolution," IEEE Signal Processing Magazine, 1996.

[12]   T. Chan, "An Optimal Circulant Preconditioner for Toeplitz Systems," SIAM J. Sci. Stat. Comp. Vol. 9, pp. 766-771, 1988.

[13]   H. C. Andrews and B. R. Hunt, "Digital Image Restoration," NJ: Prentice Hall, 1977.

[14]   R. Chan, "Toeplitz preconditioners for Toeplitz systems with nonnegative generating functions," IMAJ. Numer. Anal., Vol.11, pp. 333-345, 1991.

[15]   G. E. Trapp, "Inverse of circulant matrices and block circulant matrices," Kyungpook Mathematical Journal, Vol. 13, pp. 11-20, 1973.

[16]   G. Panci, P. Campisi, S. Colonnese and G. Scarano, "Multichannel blind image deconvolution using the bussgang algorithm: Spatial and multiresolution approaches," IEEE Transactions on Image Processing, Vol. 12, No.11 , pp. 1324-1337, 2003.

[17] V. Z. Mesarovic, N. P. Galatsanos and A. K. Katsaggelos, "Regularized constrained total least squares image restoration," IEEE Transactions on Image Processing, Vol. 4, pp. 1096-1108, 1995.

[18] A. Katsaggelos, "Digital Image Processing," Springer- Verlag, 1993.

[19] A. C. Likas and n. P. Galatsanos, "A variational approach for Bayesian blind image deconvolution," IEEE Transactions on Signal Processing, Vol. 52, No. 8, pp. 2222-2233, 2004.

[20] A. K. Katsaggelos and K. T. Lay, "Maximum likelihood blur identification and image restoration using EM algorithm," IEEE Transactions on Signal Processing, Vol. 39, No. 3, pp. 729-733, 1991.

[21] L. Landweber, "An iteration formula for Fredholm integral equations of the first kind," American Journal of Mathematics, Vol. 73, pp. 615-624, 1951.

[22] G. Panci, P. Campisi, C. Colonnese and G. Scanrano, "Multichannel blind image deconvolution using the Bussgang algorithm: spatial and multiresolutional," Vol. 12, No. 11, pp. 1324-1337, 2003.

[23] N. Galatsanos and A. Katsaggelos, "Methods for choosing the regularization parameter and estimating the noise variance in image restoration and their relation," IEEE Transactions on Image Processing, Vol. 1, pp. 322-336, 1992.

[24] F. Sroubek and J. Flusser, "Multichannel blind deconvolution of spatially misaligned images," IEEE Transactions on Image Processing, Vol. 7, pp. 45-53, 2005.

[25] G. Panci, P. Campisi, C. Colonnese and G. Scanrano, "Multichannel blind image deconvolution using the Bussgang algorithm: spatial and multiresolutional approaches," IEEE Transactions on Image Processing, Vol. 12, pp. 1324-1337, 2003.

[26] M. I. Gurelli and C. L. Nikias, " EVAM: an eigen vector based algorithm for multichannel blind deconvolution of input colored signals," IEEE Transacions on Signal Processing, Vol. 43, No. 1, pp. 134-149, 1995.

[27] G. Harikumar and Y. Bresler, "Perfect blind restoration of images blurred by multiple filters: theory and efficient algorithm," IEEE Transactions on Image Processing, Vol. 8, pp. 202-219, 1999.

[28] S. J. Reeves and R. M. Mersereau, "Blur identification by the method of generalized cross validation," IEEE Transactions on Image Processing, Vol. 1, No. 3, pp. 301-311, 1992.

[29] T. F. Chan and C. K. Wong, "Total variation blind deconvolution," IEEE Transactions on Image Processing, Vol. 7, No. 3, pp. 370-375, 1998.

[30] S. Bellini, "Bussgang techniques for blind deconvolution and restoration," In Blind Deconvolution, S. Haykin ed., Prentice Hall, 1994.

[31] H. Pai and A. C. Bovik, "On eigen structure-based direct multichannel blind image restoration," IEEE Transactions on Image Processing, Vol. 10, No. 10, pp. 1434-1446, 2001.

[32] L. Y. Shih, C. W. Barnes and L. A. Ferrari, "Estimation of attenuation coefficient for ultrasonic tissue characterization using time varying state space model," Ultrasonic Imaging, Vol. 10, pp. 90-109, 1988.

[33] L. Zhang, A. Cichocki, and S. Amari, "Multichannel blind deconvolution of nonminimum phase systems using filter decomposition," IEEE Transactions on Signal Processing, Vol. 52, No. 5, pp. 1430-1442, 2004.

[34] Y. L. You and M. Kaveh, " A regularization approach to joint blur identification and image restoration," IEEE Transactions on Image Processing, Vol. 1, No. 3, pp. 416-428, 1996.

[35] Wirawan, K. Abed-Meraim, H. Maitre and P. Duhamel, "Blind multichannel image restoration using oblique projections," Proceedings Of IEEE Sensor Array and Multichannel Signal Processing Workshop, Virginia, USA, pp. 125-129, 2002.

[36] K. H. Yap, L. Guan and W. Liu, "A recursive soft decision approach to blind image deconvolution," IEEE Transactions on Signal Processing, Vol. 51, No. 2, pp. 515-526, 2003.

[37] T. Chan and C. Wong, "Convergence of the alternating minimization algorithm for blind deconvolution," Linear Algebra and its Applications, Vol. 316, No. 1-3, pp. 259-285, 2000